High Temperature Processing Symposium 2011

7-8 February 2011
Engineering Building
Swinburne University of Technology
Melbourne, Australia

Final Program and Abstract Book

Outotec

FURNACE

onesteel

CAST
CAST Cooperative Research Centre

SWINBURNE UNIVERSITY OF TECHNOLOGY

HIGH TEMPERATURE PROCESSING SYMPOSIUM 2011
Swinburne University of Technology
7 – 8 February 2011, Melbourne, Australia

Editors

Dr M. Akbar Rhamdhani

Prof Geoffrey Brooks

Nazmul Huda

Morshed Alam

Organising Committee

Dr M. Akbar Rhamdhani – ARhamdhani@swin.edu.au
Prof. Geoffrey Brooks – GBrooks@swin.edu.au
Dr Mohammad A R Dewan – Madewan@swin.edu.au
Dr Subrat Das – Subratdas@swin.edu.au
Nazmul Huda – MHuda@swin.edu.au
Morshed Alam – MMalam@swin.edu.au
Winny Wulandari – Winnywulandari@swin.edu.au
Neslihan Dogan – NDogan@swin.edu.au
Reiza Mukhlis – RMukhlis@swin.edu.au
Behrooz Fateh – Behroozfateh@swin.edu.au
Saiful Islam – Mdislam@swin.edu.au
Abdul Khaliq – Akhaliq@swin.edu.au

Published in Australia by: Faculty of Engineering and Industrial Sciences, Swinburne University of Technology

ISBN **978-0-9806708-2-0**

HIGH TEMPERATURE PROCESSING SYMPOSIUM 2011
Swinburne University of Technology
7 – 8 February 2011, Melbourne, Australia

We wish to thank the main sponsors for their contribution to the success of this symposium

Outotec

onesteel

CAST

CAST Cooperative Research Centre

FURNACE

High Temperature Processing Symposium
Swinburne University of Technology
Engineering (EN) Building, Hawthorn Campus

Sponsored by
CAST-CRC, Furnace Engineering, OneSteel and Outotec-Ausmelt

Conference Schedule

Day 1 (7 February 2011) in EN 615

8.30 to 9.00	Registrations in 6th Floor of Engineering (EN) Building
9.00 to 9.10	Welcome by **Prof Andrew Flitman** (Acting Vice Chancellor and President, Swinburne University of Technology)

Session 1	**Chaired by: Dr M. Akbar Rhamdhani**
9.10 to 9.40	**01 – Keynote:** Prof Peter Hayes (University of Queensland) - Phase Transformations, Interfacial Processes and Reaction Mechanisms
9.40 to 10.00	02 – Mr Ross Baldock (Outotec-Ausmelt) - Hot Commissioning a Multi Stage, Variable pO_2 TSL Furnace
10.00 to 10.20	03 – Mr Nazmul Huda (Swinburne) - Applications of CFD Modelling in Smelting Industries - Some Recent Developments
10.20 to 10.40	04 – Prof Doug Swinbourne (RMIT University) - Modelling Direct to Blister Copper Smelting
10.40 to 10.55	**Coffee/Tea in EN 612**

Session 2	**Chaired by: Prof Doug Swinbourne**
10.55 to 11.25	**05 – Keynote:** Prof Shin-ya Kitamura (Tohoku University) - Improvement of Dephosphorization Reaction by Using Multiphase Slag
11.25 to 11.45	06 – Mr Ross Andrews (Outotec-Ausmelt) - Industrial Start-up and Operation of a Nickel Smelter using Outotec Ausmelt Technology
11.45 to 12.05	07 - Mr Jiang Jeff Chen (University of Queensland) – Effect of Sulphur on The Reduction Roasting Of Saprolite Ore In The Caron Process
12.05 to 12.25	08 – Dr Richard Manasseh (Swinburne) – Bubble Acoustic Emissions – A Tool for Metallurgical Process Feedback?
12.25 to 1.15	**Lunch in EN 612 (Sponsored by CAST-CRC, Furnace Engineering, OneSteel and Outotec-Ausmelt)**

Session 3	**Chaired by: Dr. Guangqing Zhang**
1.15 to 1.45	**09 – Keynote:** Mr Andrea Fontana (OneSteel) - The Modern Electric Arc Furnace in Steelmaking
1.45 to 2.05	10 – Mr Morshed Alam (Swinburne) - Study on Inclined Jetting and Splashing Phenomenon in Electric Arc Furnace Steelmaking
2.05 to 2.25	11 – Prof Paulo Santos Assis (Universidade Federal de Ouro Preto) - Studies to Determine the Use of Soapstone Wastes in the Refractory Industry
2.25 to 2.45	12 – Mr Francesco Pignatale (Swinburne) - Physical Chemistry of Protoplanetary Disks
2.45 to 3.00	**Coffee/Tea in EN 612**

Session 4	**Chaired by: Prof Geoffrey Brooks**
3.00 to 3.20	13 – Prof Cuie Wen (Swinburne) - Processing, Characterisation and Mechanical Properties of Metal Foams
3.20 to 3.40	14 – Dr Masanori Suzuki (University of Queensland) - Revision of Quasi-chemical Viscosity Model to Predict Viscosity of Molten Slag in Multicomponent Oxide Systems related to Metallurgical Processes
3.40 to 4.00	15 – Prof Geoffrey Brooks (Swinburne) – Five Key Challenges Facing Pyrometallurgy
4.00 to 4.40	Panel Discussion – **Future of High Temperature Processing Research in Australia** (Dr George Collins, Prof Markus Reuter, Dr Ivan Ratchev, A/Prof Brian Monaghan)

Close of Day 1

Day 2 (8 February 2011) in EN 715

8.30 to 9.00	Registrations in 7th Floor of Engineering (EN) Building
Session 5	**Chaired by: TBA**
9.00 to 9.30	**16 – Keynote:** A/Prof John Taylor (CAST CRC, University of Queensland) – The Dark Side of Light Metals: Dealing with Oxidation and Dross
9.30 to 9.50	17 – Dr Mark Easton (CAST CRC, Monash University) – Grain Size in Cast Light Metal Alloys: The Interdependence Model
9.50 to 10.10	18 – Dr John Grandfield (Grandfield Technology Pty Ltd) – Case Studies in Application of Mathematical Modelling to Magnesium Direct Chill Continuous Casting
10.10 to 10.30	19 – Mr Abdul Khaliq (Swinburne) - Thermodynamic Analysis of Transition Metal Borides Formation in Aluminium Melt
10.30 to 10.45	**Coffee/Tea in EN 612**
Session 6	**Chaired by: Dr. Marcus Zipper**
10.45 to 11.15	**20 – Keynote:** Dr Phil Schwarz (CSIRO) - TBA
11.15 to 11.35	21 – Dr Mahesh Prakash (CSIRO) - The Use of SPH for Simulating High Temperature Processing Applications
11.35 to 11.55	22 – Mr Michael Nagle (CSIRO) - Thermodynamic Behaviour of Metallic Impurities in Carbothermal Production of Magnesium Metal
11.55 to 12.15	23 - Ms Xijing Gloria Liu (University of Queensland) - Subsolidus Phase Equilibria of System Cu-Ca-Fe-O
12.15 to 12.35	24 – Mr Taufiq Hidayat (University of Queensland) – Thermodynamic Modelling of Copper-containing Slags
12.35 to 1.20	**Lunch in EN 612 (Sponsored by CAST-CRC, Furnace Engineering, OneSteel and Outotec-Ausmelt)**
Session 7	**Chaired by: TBA**
1.20 to 1.40	25 – Prof Paulo Santos Assis (Universidade Federal de Ouro Preto) – Use of Residual Plastic into Blast Furnaces
1.40 to 2.00	26 – Dr Guangqing Zhang (UNSW) – Efficient Utilisation of Coal by Integrating Various Industries
2.00 to 2.20	27 – Ms Giane Aparecida Silva (REDEMAT, UFOP) – Exergy Balance of Pulverized Coal Injection into Blast Furnaces
2.20 to 2.40	28 – Ms Jing Zhang (UNSW) – Effect of Impurities on Gasification of Graphite
2.40 to 3.00	29 – Mr Hazem Labib (University of Wollongong) - Flow of Liquid Slag through Coke Channels
3.00 to 3.15	**Coffee/Tea in EN 612**

Session 8	Chaired by: TBA
3.15 to 3.35	30 - Mr Ata Fallah Mehrjardi (University of Queensland) - Investigation of Freeze Linings formed during Copper Smelting
3.35 to 3.55	31 – Mr Duk-Yong Song (Tohoku University) - Influence of Density Differences and Bottom Bubbling Conditions on Formation of Metal Emulsions
3.55 to 4.15	32 - Mr Mao Chen (University of Queensland) – Viscosity Modelling for Fully Liquid Slags containing Fe_2O_3 using a Quasi-Chemical Viscosity Model
4.15 to 4.35	33 – Mr Xiaohan Wan (UNSW) – Reaction Mechanism of Carbothermal Synthesis of Silicon Nitride
4.35 to 4.55	34 - Mr Xiaoyong Xu (University of Queensland) – A Study of Tin-Based Systems for E-Waste Processing
4.55 to 5.00	CLOSING

Close of Symposium

Campus Map – Swinburne@Hawthorn

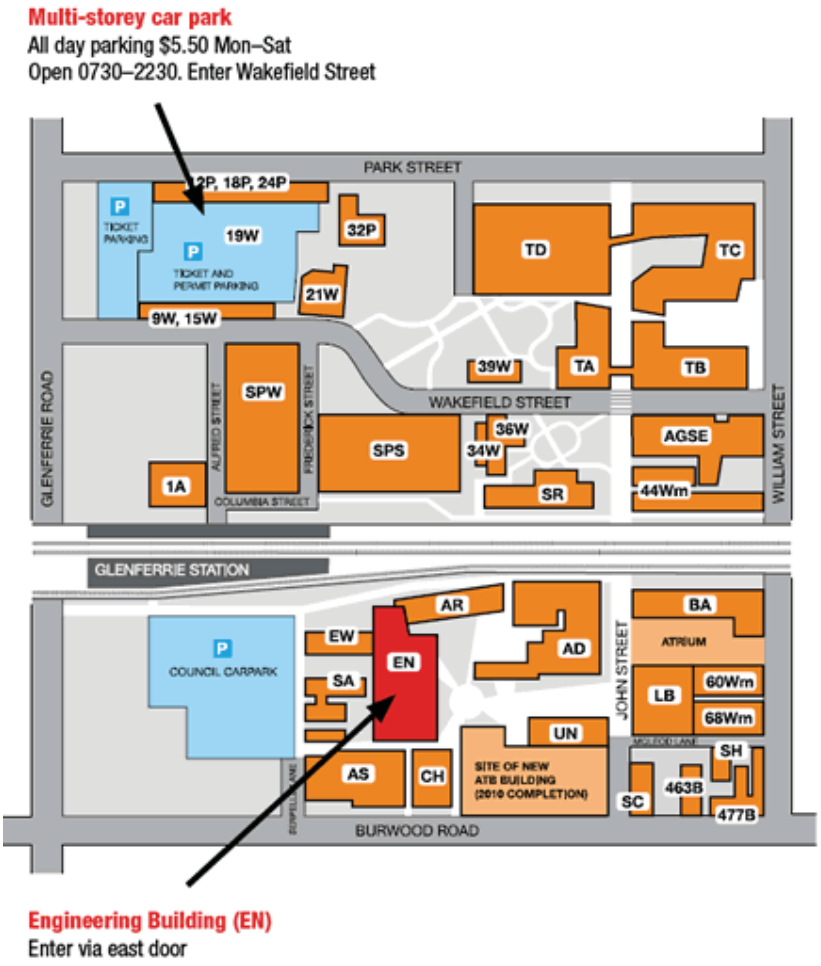

Phase Transformations, Interfacial Processes and Reaction Mechanisms

Peter C. Hayes

PYROSEARCH, Pyrometallurgy Research Centre, School of Chemical Engineering,

The University of Queensland, Brisbane, Queensland, 4072, Australia.

Keywords: Phase transformations, Reaction mechanisms, Gas/solid reactions, Solidification

Central to the practice of chemical process metallurgy and materials engineering is control of the transfer between and reorganisation of chemical species into different phases. These heterogeneous processes between gas, liquid and solid phases involve reactions occurring across and at interfaces [1-5].

The driving force for these changes is in all cases the Gibbs free energy change that will occur on moving to a new state, which is a function of temperature, bulk composition of the system and the compositions of the reactant and product phases. The condition for spontaneous change is a decrease in the Gibbs free energy of the Universe. In general we expect that the greater the difference in the initial and final states the faster the reactions will proceed.

Whilst, however, we now have a great deal of information of the Gibbs free energies of different phases much remains to be learned before we can fully understand and are able to predict the overall rates at which these heterogeneous processes proceed. The reason for this is there are many elementary processes that are simultaneously taking place during these transformations; for simplicity we can classify these processes into 4 main groups, based on similarities in their general characteristics [6]. These are:-

1. Chemical Reactions: including all forms of heterogeneous chemical reactions, occurring at the gas/solid interface, e.g. adsorption, activated complex formation and decomposition, and adsorption, desorption, decomposition reactions,
2. Nucleation/Growth: involving the appearance of metastable oxide or final metal product solid phases, and mechanisms by which species are added to those phases at gas or solid interfaces, including solid state phase transformations.
3. Mass Transport of Reactants and Products: that is, not only transport of reactant and product species in the gas phase, but also in and on condensed phases; this includes reactant species not originally present in the bulk reactant gas mixture. Transport mechanisms include bulk flow in the gas phase, diffusion in the gas phase; volume, surface and interfacial diffusion in and on the solids.
4. Physical Changes to the Reactant or Product: includes changes to product morphology taking place not only at the reaction interface during the initial product formation but also changes in the original solid material or in the product layer that could influence the overall rate or extent of decomposition of the original solid.

It is the relative rates of these individual processes determine the resultant product morphologies and the overall rates of these transformations.

In a recent analysis of the factors influencing the development of product morphologies during the gaseous reduction of metal oxides [7] the conditions for the

formation of various product morphologies were identified by considering i) established criteria for the stability of moving interfaces in a thermodynamic potential gradient, ii) the relative rates of chemical reactions on the oxide and metal surfaces, and iii) key process phenomena and physico-chemical properties of the solid phases. In the present paper these findings, and their implications for developing a more detailed understanding of the elementary process steps and mechanisms that are operative during these structural transformations, are discussed.

It has been shown [7] that the formation of product morphologies during the decomposition of metal oxides to metal in reactive gas mixtures can be understood by separately considering the behaviour of the oxide and metal phases, and the prevailing reaction conditions at the gas/oxide and gas/metal interfaces. The product morphologies are shown to, in turn, determine the rate limiting reaction steps and the kinetics of interface growth as a function of key process variables.

The selective removal of oxygen from a solid oxide surface creates a moving interface in direction z; this interface can remain planar or spontaneously become unstable forming pores in the oxide. The criteria for instability formation at the oxide surface and the transition from planar to pore growth are described by the condition,

$$\Delta G/dz < (C_{interface} - C_{bulk}).(V/D) \quad (1)$$

Increasing ($C_{interface} - C_{bulk}$) and interface velocity, V, and decreasing solute diffusivity, D, in the solid or on the solid oxide surface favours the formation of pore growth morphologies. Instability of the oxide surface is also favoured by low thermodynamic driving force for oxygen removal, ΔG.

In addition all reaction systems involving the decomposition of oxide to metal in reactive gases can be divided, to a first approximation, into three classes, depending on the relative rates of the chemical reactions on the oxide and metal surfaces.

1. If $V_o > V_m$ i.e. the rate of removal of oxygen from the surface of the oxide is greater than on the metal surface, then the oxide surface will always remain exposed to the reactive gas phase, i.e. the oxide is predominant.
2. If $V_o < V_m$, i.e. the rate of removal of oxygen from the surface of the oxide is less than on the metal surface, the oxide surface will become covered with a metal layer, i.e. the metal is predominant.
3. If $V_o = V_m$, then both oxide and metal remain exposed to the gas throughout the reaction; this corresponds to the special case of coupled or cooperative growth of metal and pores.

The condition $V_o > V_m$ can be achieved and maintained for the conditions where the oxide surface becomes unstable thus forming cellular or dendritic pores in the oxide. For cellular or dendritic pore growth the shape and velocity of the growing pore tip is determined in the limit by diffusion of excess metal solute into the bulk oxide ahead of the moving interface, however, it should be appreciated that this involves simultaneous removal of oxygen from the surface of the oxide as it moves through the bulk oxide and solid state diffusion at the pore tip.

Under conditions $V_o < V_m$ the initial metal layer is formed on the oxide surface. This layer can be maintained throughout the remainder of the reduction reaction, or the layer can periodically breakdown as a result of reactions at the metal/metal oxide interface. From a processing point of view the conditions leading to continuation of the dense metal product layer are highly undesirable since the rates become controlled by the permeability of oxygen through the metal phase. The conditions for breakdown of the metal appear to be dependent primarily on thermodynamic driving force for reduction, temperature and metal/oxide combination.

Coupled growth, when $V_o = V_m$ is highly desirable for fast reduction since continued gas access to the reaction interface is maintained throughout the reaction. The critical conditions for coupled growth depend on the stability of the oxide surfaces, but from a processing perspective appear to be principally dependent on the thermodynamic driving force for reduction. Coupled growth on stable planar and unstable oxide surfaces is favoured by high thermodynamic driving forces; under these conditions the available thermodynamic driving force can drive mass transport processes in and on the oxide and generate atomically rough oxide surfaces, both of which are necessary to sustain this product morphology.

For the reduction of metal compounds in reactive gas mixtures the conditions required to obtain the various product morphologies can be conveniently summarised on "morphology maps", of the form thermodynamic driving force, ΔG vs temperature for a given initial oxide composition and gas species in the gas mixture [6]. The methodology is shown [7] to be general, and can be applied to the analysis of any system involving the decomposition of metal compounds in reactive gas atmospheres.

Summary

Central to the practice of chemical process metallurgy and materials engineering is control of the transfer between and reorganisation of chemical species into different phases. A common feature of heterogeneous reactions between gas, liquid and solid phases is the simultaneous occurrence of many elementary processes taking place during these transformations; these processes involve both chemical reactions occurring across and at interfaces, and a range of mass transport processes.

Through examination of the reaction interfaces formed during the decomposition of oxides in reactive gas mixtures [7-10] it has been shown that the cellular and dendritic pore structures formed in reactive gas/solid oxide systems are, from a theoretical perspective, directly analogous to the solid structures formed in liquid/solid metal alloy transformations, and as such similar mathematical treatments can be used to describe these phenomena.

The identification of this fundamental link between these various classes of heterogeneous transformations offers not only the potential to develop a more generic understanding of reaction mechanisms and kinetics in these systems, but also the potential to design and better control product morphologies and reaction rates in these systems to our advantage.

References

1. Christian J.W., Theory of Phase Transformations in Metals and Alloys, Pergamon, 1965.
2. Kurz W. and Fischer D.J., Fundamentals of Solidification, 3rd ed., Trans Tech., 2004, p74, p.88, p.151.
3. Jackson, K.A., Kinetic Processes – Crystal Growth, Diffusion and Phase Transitions in Materials, Wiley-VCH, 2004.
4. Szekely, J., Evans, J.W. and Sohn, H.Y., 1976. *Gas-Solid Reactions*. Academic Press, Inc., New York.
5. Sohn H.Y. and Chaubal P.C., in *Transport Processes in Engineering* 4, Ed. Sahai Y and St.Pierre, Elsevier, pp.1-52.
6. Hidayat T., M.Phil., Metallurgical Engineering, The University of Queensland, 2009.
7. Hayes P.C., *Metal. Mater. Trans. B*, 2010, vol. 41,(1) pp.19.-34.
8. Hayes P.C., *Mineral Processing and Extractive Metallurgy Reviews*, 1992, vol.8 (1-4), pp.73-94.
9. Hidayat T., Rhamdhani A., Jak E. and Hayes P.C**.,** *Metal. Mater. Trans. B*, 2008, vol. 40B, pp. 474 -489, *ibid.* 2009, vol.40, pp.1-16. 2009, *ibid.*vol. 40B, pp. 462-473.

Hot Commissioning a Multi Stage, Variable pO_2 TSL Furnace

Ross Baldock and Ross Andrews
Outotec Ausmelt, Dandenong, VIC 3175, Australia

Keywords: Lead, Outotec Ausmelt, TSL furnace

Yunnan Tin Corporation Limited (YTCL) commissioned Ausmelt to establish a lead smelter near its existing tin operations in Yunnan province, southern China. The tin operations, already utilising an Ausmelt TSL furnace as the primary smelting vessel, was commissioned in 2002[1]. YTCL are also currently building a copper smelter based on Ausmelt TSL technology that is due for startup in 2010.

The lead project uses a single Ausmelt TSL furnace to process lead concentrates to produce 100,000 tonnes per annum of lead as crude lead bullion. The products from the Ausmelt furnace are lead bullion, a discardable slag and a zinc rich fume, all produced in a three stage batch process shown schematically below in Figure 1. The process is the same as that designed for the HZL furnace in India[2], however at a larger scale.

Smelting Stage
Lead concentrates, lead rich fume (recycle), refinery reverts and silica and limestone flux are smelted in the Ausmelt furnace to produce crude lead bullion and a lead rich slag in the concentrate smelting stage. Lead bullion was intermittently tapped from the furnace and transferred to the refinery. The bath operating temperature for the smelting process was 1100-1150°C. The lead and iron sulphides present in the concentrates are oxidised with a controlled amount of excess air injected via the Ausmelt lance. The iron oxide combines with the SiO_2, CaO, Al_2O_3 and MgO components present in the feed mix and coal ash to form a fluid slag containing approximately 30% lead as PbO. The addition of silica and limestone flux is necessary to ensure that the slag will remain fluid in the later process stages when the PbO is reduced from the slag.

While the oxidation of sulphides releases energy, supplementary energy input via fuel (fine coal) injected through the Ausmelt lance is required to maintain the bath temperature at 1100-1150°C throughout this stage. Oxygen enrichment of the lance air to ~35% was employed in this stage to reduce the offgas volume and minimise fuel requirements.

A considerable amount of fume was generated during this stage due to the volatilisation of Pb, Zn As and Sb species. This fume was collected and recycled to maximise the overall recovery of lead. Fume from the slag reduction process also had a high lead content and was recycled with the fume from the concentrate smelting stage.

Slag Reduction
The slag reduction process was commenced when the furnace was filled with slag. This stage involved reducing the lead rich smelting slag initially with additional concentrate (to ~10% Pb) and then lump coal (to ~5% Pb), to recover a lead bullion product. Fume produced from

this stage was recycled to the concentrate smelting stage. The bath operating temperature for the slag reduction stage was 1200°C.

Slag Fuming

After tapping the lead bullion product, the slag fuming process commenced. Reductant coal was fed to produce a zinc/lead fume product that was not recycled and discard slag. The discard slag was tapped from the furnace, leaving a heel for the resumption of concentrate smelting in the next cycle. The bath operating temperature for the slag cleaning stage was 1250°C.

Hot Commissioning

Following the design, construction and cold commissioning activities, the furnace heat up commenced on 17th July 2010. A very aggressive stage wise hot commissioning schedule was followed that resulted in the plant operating the process as designed at ~90% of design capacity, within 6 weeks. The hot commissioning milestones as achieved are given in Table 1 below.

Table 1: Hot Commissioning Milestones

Date	Stage
17 July	Begin Heat Up
21 July	Outotec Ausmelt arrive Lance Lit
23 July	Slag Smelting
25 July	Concentrate Smelting
29 July	Smelting 40 t/h (design rate)
31 July	Smelting and Reduction
12 August	Smelting, Reduction and Cleaning
16 August	Concentrate in Reduction
30 August	Outotec Ausmelt leave

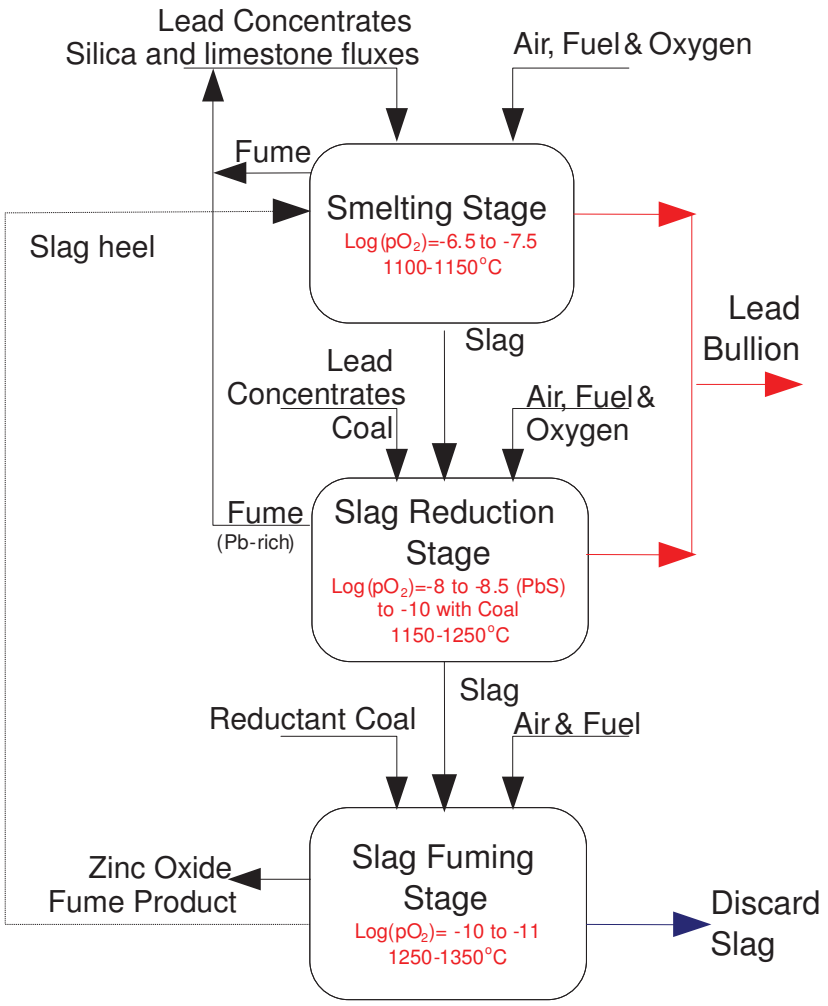

Figure 1: Process Schematic

References

1. B. R. Baldock and W. E. Short, "Australian Technology on the World Scene – Update on Ausmelt Plants and Projects", MINPREX 2000, International Congress on Mineral Processing and Extractive Metallurgy, Melbourne, Australia, September 11-13, 2000, p169-174.
2. R. A. McClelland, J Hoang, B. W. Lightfoot, D Dhanavel, "Commissioning of the Ausmelt Lead Smelter at Hindustan Zinc", Sohn International Symposium, International Symposium on Sulphide Smelting, San Diego, USA, 27-31 August 2006, pp163-171.

Applications of CFD Modelling in Smelting Industries – Some Recent Developments

Nazmul Huda[1], J. Naser[1], G. Brooks[1], M. A. Reuter[2], R. W. Matusewicz[2]

[1]Swinburne University of Technology, Hawthorn, Vic 3122, Melbourne, Australia
[2]Outotec Limited, 12 Kitchen Rd, Dandenong, Vic 3175, Melbourne, Australia

Recent advancement in the high performance computing facilities has enabled Computational Fluid Dynamic (CFD) modelling technique as a powerful tool for the researchers working in the metallurgical field. CFD can predict flows ranging from simple single phase flows to complex multiphase flows in high temperature combusting environment associated with metallurgical process and smelting industries. Successful and efficient development of a CFD model can predict the fluid flow behaviour, combustion behaviour, generation of turbulence and splashing and other fluid dynamic parameters inside the furnace. Present authors have developed a CFD model for zinc slag fuming process for top submerged lance smelting furnace. The model integrates complex combustion phenomena and chemical reactions with the heat, mass and momentum interfacial interaction between the phases present in the system. The model is based on 3-D Eulerian multiphase flow approach and commercial CFD package AVL FIRE 2009.2 (AVL, Graz, Austria) coupled with a number of user defined subroutines (UDF) in FORTRAN programming language were used to develop the model. The model predicted the velocity and temperature field of the molten slag bath, species mass fractions for CO, CO_2, H_2O, CH_4, O_2 and N_2, generated turbulence, vortex and plume shape at the lance tip. Effect of lance submergence level on zinc fuming rate were investigated with the model by using three different submergence levels (H'/L' = 1/5, 1/4 and 1/3). The model predicted that overall zinc fuming rate for 1/3 lance submergence level is 1.3 times higher than 1/5 lance submergence level. The model was applied to rectangular zinc fuming furnace with submerged tuyers and ran successfully. The model is a significant advancement for further research in smelting industries by using CFD tool.

Figure 1 shows the schematic diagram of the modelled TSL furnace. Figure 2 shows the volume fraction distribution for molten slag phase of the transient simulation. Figure 2(a) shows the cross sectional view of the volume fraction on the vertical X-Z plane. The generated plume shape at the lance tip due to gas injection and combustion is clear from this figure. Figure 5(b) shows the 3D view of the generated splashing inside the furnace.

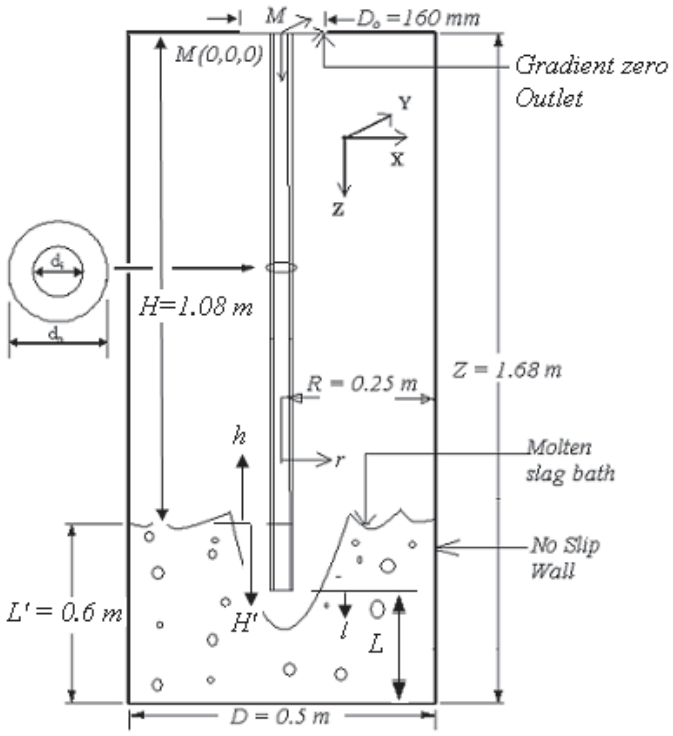

Figure 1: Schematic diagram of the modelled TSL furnace

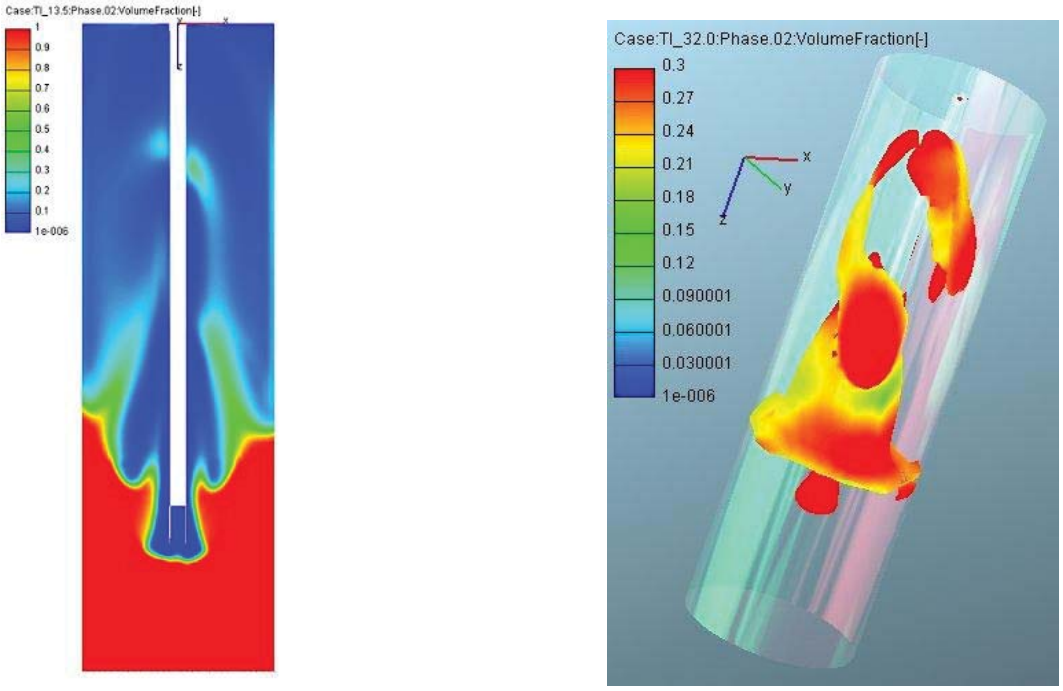

(a) (b)

Figure 2: Volume fraction distribution for molten slag phase only (a) Cross section view along X-Z plane, (b) 3D view of generated splash above the bath

Modelling direct to blister copper smelting

Prof. Doug Swinbourne
RMIT University, Melbourne

The most important mineral of copper is chalcopyrite $CuFeS_2$ and ores containing it are upgraded by flotation to concentrates containing from 30–35 wt-% Cu. Modern smelting practice often uses the Outotec flash smelting process. Dry concentrate with air and silica flux is sprayed into a vertical reaction shaft which is at approx. 1300°C. Slag and matte particles form and drop into the settler where phase separation takes place. Matte is transferred to a Peirce-Smith converter, silica flux is added and air is injected until the matte is essentially molten Cu_2S, then it is further oxidised without fluxes to molten 'blister copper'. Outokumpu showed in the 1960's that any copper concentrate could be smelted directly to copper in a flash furnace, bypassing matte converting, but that with chalcopyrite the amount of slag formed was so great that the copper recovery was too low to be economic. Some copper orebodies contain minerals with much lower iron contents e.g. bornite Cu_5FeS_4 and chalcocite Cu_2S. Smelting them produces much less slag so copper recoveries will be higher and the process becomes economic. In this work the smelting of a concentrate whose composition varies from bornite to chalcopyrite will be modelled. It will be shown how entrainment of copper-bearing material in the slag can be accommodated in a thermodynamic model. Finally, the effect of changing the slag composition on key process variables will be examined. The HSC Chemistry for Windows v.5.1 software package was used and activity coefficients of all species obtained from the literature. The basis of calculation was 1000 kg of concentrate and the amount of silica flux used was that required to produce a final slag with a Fe/SiO_2 ratio of 2. The oxidising gas was assumed to be 70% O_2(g) and the temperature was 1300°C. Copper recovery to blister copper is shown in the first figure while the relationship between the copper content of the slag and the sulphur content is given on the next. In practice the copper content of the slag is higher than equilibrium due to the entrainment of unoxidised $CuS_{0.5}$. This can be simulated by introducing"Cu" into slag and giving it a suitable activity coefficient value. Copper recovery decreases to only a little over 50% when chalcopyrite is smelted.

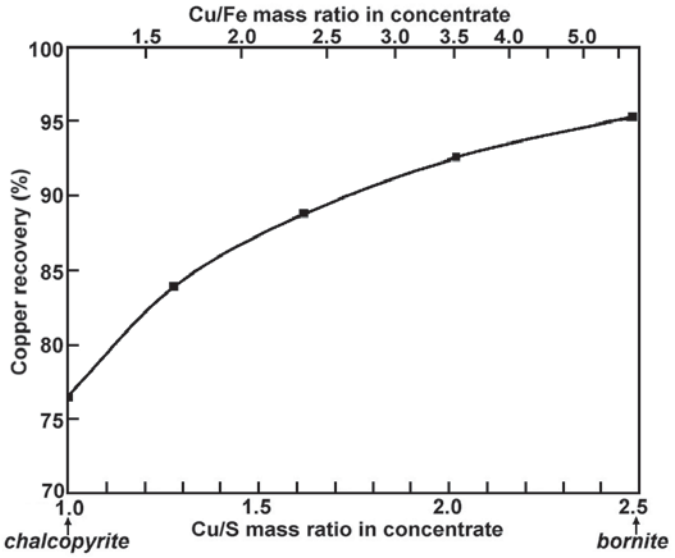

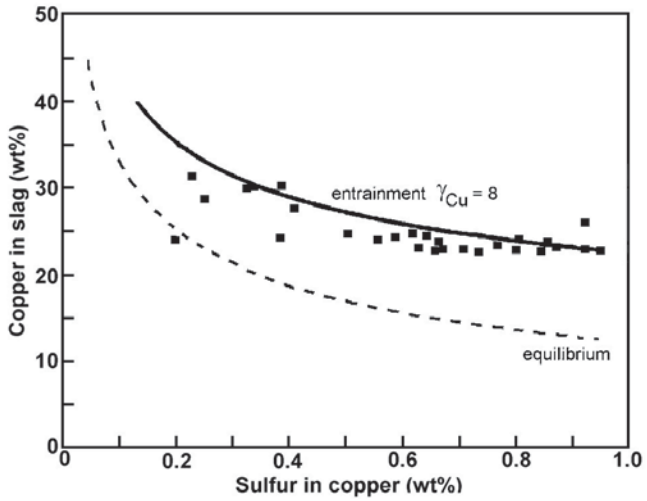

Slag composition controls copper recovery because it determines the activity coefficient of $CuO_{0.5}$ in the slag and the slag mass. Takeda presented activity coefficient data for $CuO_{0.5}$ in SiO_2-CaO-MgO-FeO_x slags as 1300°C and this data was used to show the affect of changing the fluxing of the slag. As expected, the dissolved copper content of the slag decreases as the activity coefficient of copper increases, but the entrained copper content remains almost constant. The recovery of copper becomes a maximum at an activity coefficient of $CuO_{0.5}$ of 4. Thereafter the copper recovery drops because the slag mass rapidly increases while the copper content of the slag is decreasing only slowly.

References

A. G. Hunt, S. K. Day, R. G. Shaw and R. C. West: 'Developments in direct-to-blister smelting at Olympic Dam' Proc. Int. Conf. 'Copper 99 – Cobre 99', (ed. D.B. George *et al.*), Phoenix, Arizona, 239-253; October 1999, Warrendale, PA, TMS.

Y. Takeda (1994): 'The effects of basicity on oxidic dissolution of copper in slag', Proc. Int. Symp. 'Metallurgical processes for the early twenty-first Century', Vol.1 'Basic Principles', (ed. H.Y. Sohn), San Diego, California, 453-466; September 1994, Warrendale, PA, TMS.

Improvement of Dephosphorization Reaction by Using Multiphase Slag

Shin-ya Kitamura, Farshid Pahlevani, Nobuhiro Maruoka and Hiroyuki Shibata
Tohoku University, 2-1-1 Katahira, Aoba-ku, Sendai, Japan

Key words: dephosphorization, slag, BOF, reaction kinetics, simulation:

1. Introduction

In most cases, steelmaking slag and hot metal dephosphorization slag are in a solid-liquid coexisting states containing dicalcium silicate as the solid phase. From the phase diagram of the CaO-SiO_2-P_2O_5 system, it is well known that dicalcium silicate (C_2S) and tricalcium phosphate (C_3P) form a solid solution at the steelmaking or hot metal dephosphorization temperature in a wide composition range[1]. This phase diagram implies that the main products of the dephosphorization reaction can be dissolved into the main solid phase in the slag. Ito et al.[2] have observed large partition ratio of phosphorus between liquid slag and the solid solution of C_2S and C_3P. According to this result, it can be said that phosphorus is more stable in the solid solution than in the liquid slag phase. The authors have proposed a new dephosphorization model that takes into account the solid phase in the slag[3].
In order to utilize the solid solution efficiently, the rate of phosphorus enrichment from liquid slag to the solid solution and the partition ratio of phosphorous between liquid slag and the solid solution should be clarified for various slag conditions. To meet this requirement, the fundamental experiments were conducted. Combining these results with the model, some aspects to improve the dephosphorization in steelmaking process were clarified.

2. Phosphorus enrichment rate from liquid slag to the solid solution.

By the change in composition or temperature during refining, the solid solution of C_2S-C_3P directly precipitates from the liquid slag. In a previous study, we measured the mass transfer

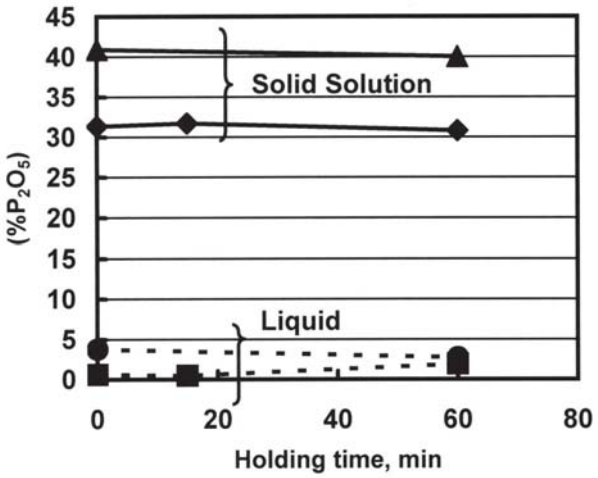

Figure1 Change in P_2O_5 content in solid solution and liquid phase with holding time.

rate of phosphorous[4]. About 0.2g of the melted slag was cooled from 1873 K to 1473 K in Pt crucible. The composition of the slag was adjusted so as to precipitate the solid solution during cooling from the liquid slag. After holding at 1473K for various times, the slag was quenched, the partition ratio of phosphorous was measured. The result is shown in Figure 1

and it was found that the distribution ratio reached equilibrium conditions, irrespective of the time at 1473 K; and it was clarified that the mass transfer rate was very fast.

3. The partition ratio of phosphorous between liquid slag and the solid solution

The authors have studied the effect of P_2O_5 content and the influence of oxides such as MgO, MnO and Al_2O_3 on the partition ratio in the CaO-SiO_2-FeO_x-P_2O_5 slag system[4,5]. As the liquid slag and solid solution are in the equilibrium, the activity of P_2O_5 in solid solution and liquid phase are the same. Then, the observed distribution ratio is proportional to the activity coefficient of P_2O_5 in each phase, as shown in equation 1. Where a is the activity; γ, is the activity coefficient; and k, is the coefficient for the conversion of mass percentage to mol fraction. Subscripts P_2O_5 (Liq) and P_2O_5 (SS) denote the activity and activity coefficient of P_2O_5 in the liquid phase and the solid solution, respectively.

$$L_p = \frac{(\%P_2O_5)_{SS}}{(\%P_2O_5)_L} = k\frac{a_{P_2O_5(SS)} \times \gamma_{P_2O_5(L)}}{a_{P_2O_5(L)} \times \gamma_{P_2O_5(SS)}} = k\frac{\gamma_{P_2O_5(L)}}{\gamma_{P_2O_5(SS)}} \qquad (1)$$

As the activity of P_2O_5 in the liquid phase is calculated by a regular solution model, the activity coefficient of P_2O_5 in solid solution is able to be evaluated. By this study, the authors have found that the activity coefficient of P_2O_5 in solid solution was influenced by P_2O_5 content and the content of the oxide other than CaO, SiO_2 and P_2O_5 in solid solution (solved oxide). By the regression analysis, the following empirical equation was obtained, where W is the total solved oxide content.

$$log\gamma_{P_2O_5(SS)} = 0.0409 \times (\%P_2O_5)_{SS} + \left(1.4305 \times W^{1/2} - 17.567\right) - 1.227 \qquad (2)$$

The activity coefficient of P_2O_5 in liquid slag is considered to be governed by CaO content in liquid phase and that in solid solution is described in equation (2). Therefore, the partition ratio can be controlled by these factors. Figure 2 shows the relation between partition ratio of P_2O_5 and CaO content of liquid phase in different activity coefficient of P_2O_5 in solid solution. Fairly good relation was obtained.

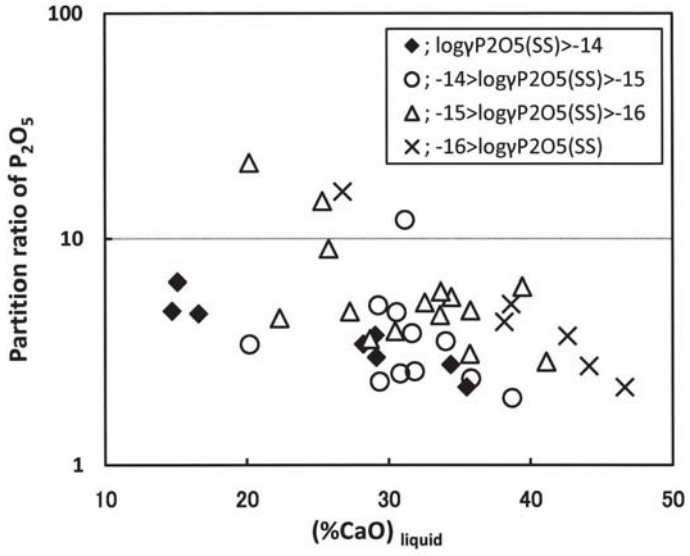

Fig.ure 2 Relation between partition ratio of P_2O_5 and CaO content in liquid slag at different activity coefficient of P_2O_5 in the solid solution.

4. Simulation model of hot metal dephosphorization by multiphase slag

The authors have proposed a new hot metal dephosphorization model that taken into account the solid phase in the slag and the dissolution rate of the flux[3]. In this model, three phases—solid slag, liquid slag, and liquid metal—and the reaction between the solid and liquid slag

are considered besides the reaction between the liquid slag and liquid metal. A coupled reaction model[6] is used to calculate the reaction kinetics between the molten slag and metal phases. When C_2S is precipitated in slag, the P_2O_5 content is distributed between the solid and liquid phases based on the equilibrium partition ratio[5]. But when the other solid phase is precipitated, P_2O_5 is pushed out into the liquid phase. To calculate the dissolution rate of lime, empirical equation, assuming that the dissolution rate is controlled by the mass transfer in the slag is used. The calculated results are in good agreement with the experimental results for various slag compositions and methods of flux and oxidizer addition. The precipitation or dissolution of solid solution during refining is influenced by the change in basicity, FeO content and temperature. Therefore, the dephosphorization behaviour is greatly depends on the change in the fraction of solid solution in slag as shown in Figure 3. With this simulation

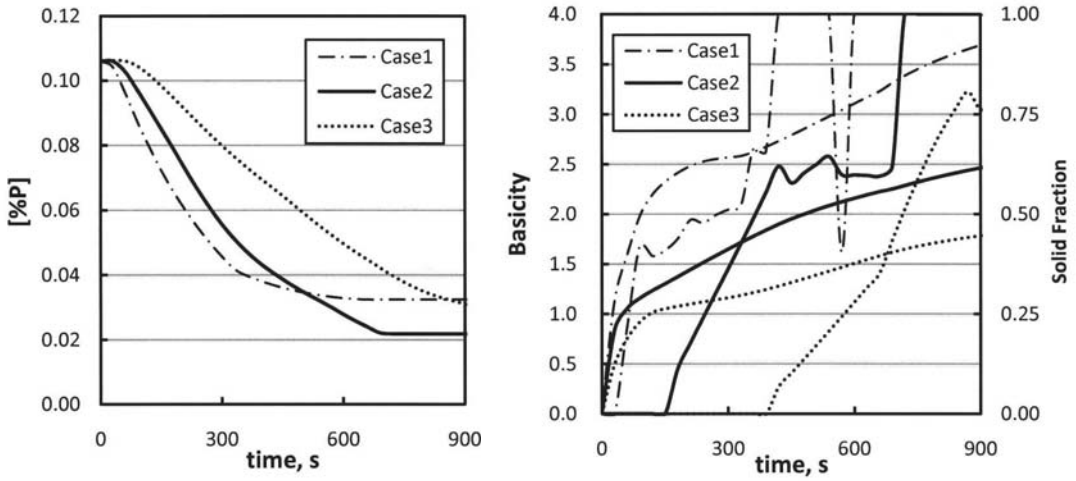

Figure 3 Change in dephosphorization behaviour, basicity and fraction of solid solution in slag during refining.

model, the influence of various factors on the reaction efficiency can be discussed.

References

1. W. Fix, H. Heymann, and R. Heinke, *J. Am. Ceram. Soc.*, 52 (1969), pp.346–347.
2. K. Ito, M. Yanagisawa, and N. Sano, *Tetsu-to-Hagan*e, 68 (1982), pp.342–344.
3. Shin-ya Kitamura, Ken-ichiro Miyamoto, Hiroyuki Shibata, Nobuhiro Maruoka and Michitaka Matsuo, *ISIJ International*, 49(2009), pp.1333-1339.
4. Ken-ichi Shimauchi, Shin-ya Kitamura and Hiroyuki Shibata, *ISIJ International*, 49(2009), pp.505-511.
5. Farshid Pahlevani, Shin-ya Kitamura, Hiroyuki Shibata and Nobuhiro Maruoka, *ISIJ International*, 50(2010), pp.822-829
6. S. Ohguchi, D.G.C. Robertson, B. Deo, P. Grieveson and J.H.E. Jeffes, I*ronmaking and Steelmaking*, 11 (1984), p.202-213.

Industrial Start-up and Operation of a Nickel Smelter using Outotec's Ausmelt Technology

Ross Andrews
Outotec, Dandenong, VIC 3175, Australia

Keywords: Nickel, Outotec, Ausmelt, TSL furnace

A second commercial nickel smelter using Outotec's Ausmelt technology (and JAE nickel smelting technology) was commissioned in China in November 2009. Despite some initial set backs in productivity and equipment, the plant has achieved design with respect to matte grade and smelting capacities. This presentation provides some details of the commissioning of this nickel smelting project and in particular it presents some contrast to the smooth and successful commissioning of the JNMC nickel smelter in September 2008, presented at the 2010 High Temperature Symposium.

Extended Abstract

A second commercial nickel smelter using Outotec's Ausmelt technology (and JAE nickel smelting technology) was commissioned in China in November 2009. Despite some initial set backs in productivity and equipment, the plant has achieved design with respect to matte grade and smelting capacities. This presentation provides some details of the commissioning of this nickel smelting project and in particular it presents some contrast to the smooth and successful commissioning of the JNMC nickel smelter in September 2008, presented at the 2010 High Temperature Symposium.

The Ausmelt Furnace was designed to treat 249,000 dry tpa of nickel-copper concentrates and 18,600 dry tpa of other nickel bearing material in a continuous smelting operation.

In the nickel smelting process, a proportion of the sulphides in the nickel concentrates are oxidised with a controlled amount of air and oxygen injected via the Ausmelt lance. The iron oxide formed combines with the SiO_2, CaO, Al_2O_3 and MgO components present in the feed mix and coal ash to form a slag. If required, additional fluxes are added to ensure a fluid slag. Sulphur dioxide is generated as a product of the oxidation reactions and leaves the furnace together with other gaseous components. The slag, low in Cu and Ni is discarded after settling in an ESF, whilst the nickel-copper matte is further processed. As high levels of MgO can be present, operating temperatures up to 1400°C are used.

The commissioning of this furnace was quite a different experience when compared with the commissioning of the JNMC process the year previous. Some of the hurdles during the commissioning process are discussed in this presentation.

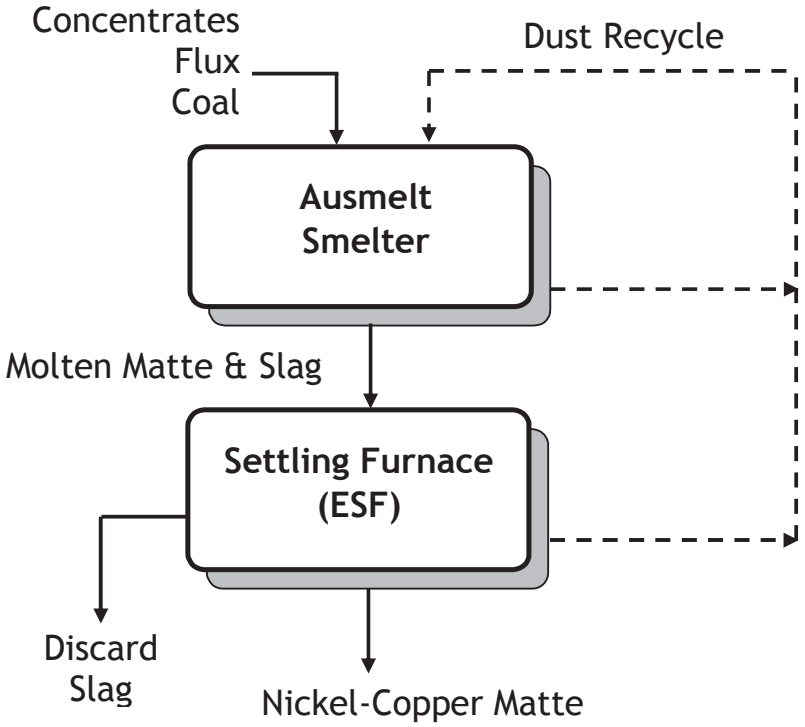
Concentrates
Flux
Coal
Dust Recycle
Ausmelt
Smelter
Molten Matte & Slag
Settling Furnace
(ESF)
Discard
Slag
Nickel-Copper Matte

Effect of Sulphur on The Reduction Roasting Of Saprolite Ore In The Caron Process

J.Chen, E.Jak, P.C.Hayes

Pyrometallurgy Research Centre, School of Engineering, The University of Queensland, Brisbane QLD 4072, Australia

Key Words: Saprolite; Reduction Roasting; TEM; SEM; XPS

The Caron process, which involves reduction roasting of the ore followed by ammonical leaching of reduced ore, has been successfully used in processing the iron-rich limonitic part of the nickel laterite ore body. Reserves of limonite ores are however limited and there are large deposits of saprolitic ores (with high Mg and Si content) that cannot currently be economically processed by the Caron process. Previous laboratory investigations on the treatment of saprolite ore using the Caron process have found significant improvement in nickel extraction by the addition of S during the reduction roasting stage; however, plant trials have shown negligible effect on nickel recovery with addition of S.

Recent research on the reduction roasting of saprolite ore, utilizing modern analytical skills and equipment to reveal mechanisms of reduction of nickel from Saprolite with S addition and how this process is controlled by accompanying reactions or transformations.

Handpicked Saprolite rocks consisting of 97% of Serpentine (Lizardite) supplied by QNI Yabulu Refinery was ring milled and sieved to obtain portion with particle size less than 38 μm as starting material. Reduction roasting experiments were carried out in a fluidised-bed reactor. Saprolite samples were treated at temperature between 150^{o}C to 800^{o}C in 15%H_2/N_2 gas mixtures with addition of 1%wt of elemental sulphur. Reduced samples were sent to QNI Yabulu Refinery for leaching test and chemical analysis. Small portions of reduced ore were reserved for X-ray powder diffraction (XRD), Scanning Electron Microscope (SEM), Transmission Electron Microscope (TEM) and X-ray Photoelectron Spectroscopy (XPS) analysis.

Great improvement in Ni recovery by ammonical leaching after reduction roasting has been demonstrated with addition of S at temperatures below 600^{o}C and at 800^{o}C with maximum nickel recovery of 92% obtained at 600^{o}C. It has been revealed by XPS analysis that added elemental S quickly adsorbed on the ore surface in the form of sulphate when temperature is above 150^{o}C; this process is essential for stabilization of S and preventing it from vaporization at high temperatures. Combined TEM and EDS analysis indicated that a Ni sulphide phase forms at temperature as low as 350^{o}C, presenting a different reaction mechanism to the formation of Ni-Fe alloy nano-particles takes place above 500^{o}C when no S is added[1]. SEM and BET analysis shown that Olivine densification is suppressed by S at high reduction temperatures (i.e. 800^{o}C).

Possible mechanisms have been proposed to explain improved Ni recovery with S addition in reduction roasting stage.

1. At low reduction temperature (below 600^{o}C), Ni sulphide forms at much lower temperature and becomes accessible to leaching; while when no S is added, the extent of formation of leachable Ni bearing phase - Ni-Fe alloy is controlled by the extent of dehydroxylation of Saprolite which takes place mainly between (500^{o}C-700^{o}C)

2. At high reduction temperature (750^{o}C-800^{o}C), the suppressed olivine densification by S has reduced effect of the encapsulation of formed Ni-Fe alloy nanoparticles[1], therefore, leachable Ni bearing phase becomes more accessible to leaching

References

1. J. Chen, et al., "Factors Affecting Nickel Extraction From the Reduction Roasting of Saprolite Ore in the Canon Process", *Pyrometallurgy of Nickel and Cobalt 2009-Proceedings of the International Symposium*, pp. 449-461.

Bubble-Acoustic Emissions - a tool for Metallurgical Process Feedback?

Richard Manasseh[1,2,3]

[1]Faculty of Engineering & Industrial Science, Swinburne University of Technology
[2]Fluid Dynamics Group, CSIRO
[3]Department of Mechanical Engineering, University of Melbourne

Keywords: Bubble; Acoustic; Emission; Sound; Metallurgy; Process; Feedback

Bubbles are sparged into molten metals in several metallurgical processes. Audible and often very loud sounds are generated by the formation and volumetric vibration of bubbles. Anedoctal evidence from plant operators is that there is a relation between the perceived quality of these noises and the process performance. However, translating this concept to practice is challenging[1] and should benefit from a deeper understanding of the physics of bubble sound emission.

The fundamentals of bubble sound emission are presented, beginning with the emissions of precisely-generated individual bubbles. Bubbles vibrate volumetrically because gases are compressible, providing a spring, while the surrounding liquid is a mass[2,3]. The resulting spring-mass system is a natural mechanical oscillator: the bubble 'rings' like a bell on formation or following other topological changes like breakup or coalescence[4]. Acoustic emissions of bubble chains[5] and plumes and finally of highly turbulent, complex bubbly flows[6,7] are presented.

Measurement hardware and systems appropriate for high-temperature operations are presented. Issues in relating the measured sound frequencies to the bubble size are discussed. The output of a carefully windowed and processed passive bubble-acoustic signal stream is shown to consist of two useful elements: the rate of bubble production, and the bubble size[7,8]. Finally, applications to metallurgical processes are projected.

References

1. J. W. R. Boyd and J. Varley. The uses of passive measurement of acoustic emissions from chemical engineering processes. *Chem. Eng. Sci.*, 56:1749–1767, 2001.
2. M. Minnaert. On musical air bubbles and the sound of running water. *Phil. Mag.*, 16:235–248, 1933.
3. T. G. Leighton. *The Acoustic Bubble*. Academic Press, London, 1994.
4. Manasseh, R., Riboux., G. & Risso, F., 2008, Sound generation on bubble coalescence following detachment. *International Journal of Multiphase Flows* 34, 938–949.
5. Nikolovska, A., Manasseh, R. & Ooi, A., 2007, On the propagation of acoustic energy in the vicinity of a bubble chain. *Journal of Sound and Vibration* 306, 507–523.
6. Chanson, H. & Manasseh, R., 2003, Air entrainment processes in a circular plunging jet: void-fraction and acoustic measurements. *Journal of Fluids Engineering* , Trans. ASME, 125 (5), Sept. 910–921 (ISSN 0098-2202).
7. Manasseh, R., Ooi, A., 2009. Frequencies of acoustically interacting bubbles. *Bubble Science, Engineering and Technology* 1 (1-2), 58-74.
8. Manasseh, R., LaFontaine, R. F., Davy, J., Shepherd, I. C. & Zhu, Y., 2001, Passive acoustic bubble sizing in sparged systems. *Experiments in Fluids* 30 (6), 672–682.

The Modern Electric Arc Furnace in Steelmaking

Andrea Fontana
OneSteel, Laverton North, VIC 2026 Australia

Key words: EAF technology, EAF safety, EAF process control

Since its introduction in the 1960s, Electric Arc Furnace (EAF) steelmaking evolved rapidly from a boutique technology to the second largest steelmaking technology behind the traditional Basic Oxygen Furnace (BOF)[1]. In 2010, the amount of steel produced via the EAF route was 389 million tonnes, out of a total steel production of 1.39 billion tonnes, i.e. 28% of the total amount[2].

In principles, arcs in steelmaking furnaces are similar to welding arcs but increased enormously in power. In an EAF the arc voltage ranges between 100 and 800 V and currents between 10 and 150 kA. Active power greater than 100 MW is quite common for large furnaces these days[3].

The key of the EAF success can be summarised in one word: flexibility. Recycled steel scrap is historically the main raw material, saving the consumption of virgin iron ore, but basically any type of material with relevant iron units can be used as an input (e.g. DRI, HBI, liquid iron). A wide range of final products can be made via the EAF route, from plain carbon steel to high-alloy steel. The batch capacity of an EAF varies depending on its size (normally between 50 and 300 tonnes) and power input, with production rates reaching 320 tonnes per hour[4].

The EAF design has significantly changed in the past ten to fifteen years. Furnaces grew in size, power input rates increased, and faster furnace movements were ensured in order to reduce idle time[5]. Process automation and control has also improved dramatically, with the aim of delivering process repeatability, greater productivity and higher safety standard.

In terms of market tendency, three are the types of EAFs preferred by steelmakers currently investing in a new melt shop, the main drivers being safety, productivity and total output[4]:

- Standard EAF (2, 3, 4 buckets charging);
  - main pros: high market share, reliable design, maintenance friendly, proven technology, no restriction in raw material, complete tap weight and quality range, lower investment cost;
  - main cons: limited power input, power-off time.

- Enlarged EAF (single bucket charging);
  - main pros: reduced power-off time, flexibility in scrap mix and raw materials, reliable design, maintenance friendly, use of proven technology, highest power input and yield of chemical energy due to larger shell diameter and scrap preheating taking place inside the furnace;
  - main cons: higher electrical network power required, higher flicker generation.

- Continuous scrap feeding EAF (Consteel);
    - main pros: reduced power-off time (no bucket charging), lower investment in flicker compensation (working in flat bath conditions most of the time), better environmental condition, scrap preheating;
    - main cons: scrap handling equipment needed (additional investment required), maintenance needed in the conveyor area, extensive hot heel necessary, reduced refractory life, layout restrictions due to conveyor arrangement, limitations in scrap mix (i.e. density control).

An EAF consists in a refractory-lined hearth, a wall made of water-cooled panels and a water-cooled roof on top. Graphite electrodes are used to convey the high current input. Their number varies depending on the electrical setup (AC, single DC, twin DC). Conductive arms are used to hold the electrodes. Hydraulic systems regulate the electrode movement and all other movements in general.

Recent developments in EAF technology were made in the following areas in particular[4]:

- Fixed wall-mounted burners and injectors for chemical energy input and slag foaming:
    - Burners with up to 5 MW rated power;
    - Supersonic oxygen injection for decarburisation and slag foaming;
    - Carbon injection for recarburisation and slag foaming;
    - Slag builders injection (lime, magnesia, dolomite).

- By-products and recycled materials reutilisation:
    - Recycling of used steelmaking refractories (furnace and ladle bricks);
    - Recycling of secondary steelmaking slags;
    - Usage of recycled plastics and rubber as foaming slag agent[6].

- Extensive usage of automated machines and robots to eliminate human exposure to hot work:
    - Slag door cleaning machine;
    - Tap hole opening auto-lance;
    - Tap hole cleaning auto-lance;
    - Taphole automatic sand refilling machine;
    - Temperature and sample taking robot.

- Extensive usage of infrared technology and high speed cameras:
    - Infrared slag detection system for tapping stream;
    - High resolution video cameras to control taphole filling and process monitoring in general.

- Process control equipment:
    - Off-gas online analysis and dynamic control;
    - Slag foaming detection and control;
    - Fast electrode regulation system.

- Data analysis:

  In a modern steel plant, a vast amount of data is constantly being collected by various acquisition systems (e.g. PLC, SCADA), but only a small fraction of this data is properly analysed to obtain useful information on the steelmaking process. Recent

developments in data collection and analysis aim at transforming the huge amount of production data available into information useful to increase process knowledge. Modern multi-dimensional analysis tools and techniques such as data mining find correlations and dependencies among the great number of different variables assist decision-making[7].

References

1. Brooks, G. (2001). Developments in Electric Arc Furnace Steelmaking. *Innovative Technologies for Steel and other Materials*, COM, 81-91.
2. Global Steel Update (2011, June). GrafTech.
3. Bowman, B. & Krüger, K. (2009). *Arc Furnace Physics*. Düsseldorf: Verlag Stahleisen.
4. Danieli Technology Book (2010). Buttrio, Italy.
5. Fruehan, R. J. et al. (1998). *The Making, Shaping and Treating of Steel* (11th ed.). Pittsburgh: Carnegie Steel Company.
6. Sahajwalla, V. et al. (2009). Environmentally Sustainable EAF Steelmaking through Introduction of Recycled Plastics and Tyres: Laboratory and Plant Studies. *Iron and Steel Technology*, 43(6), 43-50.
7. Morsut, L. (2010). MORE Intelligence: An Innovative Multi-dimensional Data Analysis System for Metallurgical Processes. *Steel Tech*, Vol. 2. Kolkata.

Study on inclined jetting and splashing phenomenon in Electric Arc Furnace Steelmaking

Morshed Alam[1], Gordon Irons[2], Jamal Naser[1], Geoffrey Brooks[1] and Andrea Fontana[3]

[1]Faculty of Engineering and Industrial Sciences, Swinburne University of Technology, P.O. Box H-38, Hawthorn, Victoria 3122 Australia. Email: mmalam@swin.edu.au

[2]Steel Research Centre, McMaster University, 1280 Main Street West, Hamilton, Ontario L8S4L8

[3]One Steel Laverton, 105-123 Dohertys Road, Laverton North, Victoria 3026, Australia

In Electric Arc Furnace (EAF) steelmaking, scrap metal is melted by using electric arc and oxy-fuel burner inside the furnace. After that the molten metal is purified by blowing oxygen supersonically into the molten metal which in turn results in splashing of liquids melt on the wall of the furnace. The splashed metal droplets cause wear of furnace wall and loss of production. Optimization of the operating condition (lance angle, lance height and flow rate) may allow less splashing and increase productivity. In the present study, air was injected on water surface in a small-scale model at different lance angles, lance heights and flow rates. Splashed liquid in the forward direction was collected and measured in each case. The forward splashing rate was found to increase with the increase of lance angle from the vertical and flow rate. But the splashing rate is not a monotonous function of lance height. Splashing rate increases with lance height up to a critical distance and after that splashing rate decreases with the increase of lance height. The shape of the cavity was carefully observed by using a video camera and it was found that the splashing was minimum when the cavity was operating in penetrating regime. The critical depth of penetration of water at different lance angle was measured at constant lance height. The critical depth of penetration was found to decrease with the lance angle. A correlation was obtained to determine the critical depth of penetration at different lance angles. Using the values of critical depth of penetration at different lance angle, the Blowing number[1] equation can be corrected to calculate the blowing number at different lance angles. The present study shows that the Blowing number on liquid surface increases with jet angle.

References

1. Subagyo, et al., *Generation of Droplets in Slag-Metal Emulsions through Top Gas Blowing.* ISIJ International, 2003. **43**(7): p. 983-989.

Studies to determine the use of soapstone wastes in the Refractory industry

Paulo Santos Assis [(1)], Ana Beatriz da Silva[(2)], Ludimila Melo Viana [(3)], Rômulo Alves dos Santos[(4)]

[1] UFOP, Full Prof.of Escola de Minas-UFOP, Prof at REDEMAT, Honorary Prof by HUST, China, assis@em.ufop.

[2] Federal University of Ouro Preto – Escola de Minas – UFOP, M.Sc. at REDEMAT, Ouro Preto, Brazil. E-mail beatrix08@oi.com.br

[3] Metallurgical Engineer, Grad. Student at REDEMAT, ludimilamelo@ymail.com.

[4] Metallurgical Engineer from Escola de Minas, alves_romulo@yahoo.com.br.

Universidade Federal de Ouro Preto - UFOP /Escola de Minas - Departamento de Engenharia Metalúrgica e de Materiais Campus Morro do Cruzeiro - Ouro Preto _ MG/ Brasil

The use of soapstone is traditional in the region of Ouro Preto and Mariana. It has been used for the manufacture of handmade decorative and utilitarian since colonial times. This process is rudimentary and the wastes are considered a serious environmental impact. Based on this, the objective of this work is to verify the possibility of using such waste in the manufacture of refractories, ceramics that are capable of withstanding high temperatures without losing its physical and chemical properties, including resistance, low thermal and electrical conductivity.

The methodology began with a literature about the technological characterization of residual soap stone and refractory materials, followed by the experimental part.

Firstly, a sample of 20 kg of soapstone was removed from a mining near the town of Ouro Preto in powder form, after this sample was burnt. The raw material was subjected to a grinding, and then a operation to get the fractions.

The material sieved to 400 # used only the product through and then added the binder (PVA) at a dilution of 1% (per 100 ml of water heated to approximately 100 degrees, we used a gram of the binder) to mixture was performed at a rate of 135 g of powder of soap stone (PPS) to 41 ml. The PVA has the purpose of agglutination, influencing the resistance of the resulting material. Soon then after mixing the powder and homogenized manually was brought to the oven at about 100 ° C for 48 hours for drying before the formation of the sample of cylindrical shape with about 2 cm in radius. For each sample was used about 8 grams of the material through pressure. The masses were subjected to a uniaxial compression with more than one action of the piston. The pressure applied of approximately 300 kg /cm ^{2}.

The step of burning was in electric furnace, with temperatures of 400, 600, 800 and 1,000 ^oC, where they remained for two hours analyzing its sintering and subsequent determination of resistance to compression. Soon after the calculation of density and porosity by the method of BET, where there was the hint to use the wastes to produce refractory samples.

The results obtained after the characterization of the dust of soapstone were as follows. Table I shows some results concerned to strength related to temperature treatment. Table II shows the porosity and real density.

- Mineralogical composition (volume%): 87.9% steatite, 8.7% dolomite, 3.2% chlorite, 0.2% opaque minerals;
- Structure: compact, thin, with dolomite's crystals dispersed of 2- 8 mm in diameter;
- Impact resistance: 57cm height of rupture;
- Fire resistance: undisturbed until 440 ° C.
- Its strength and hardness can be compared to the marble, with the advantage of being refractory, supporting high temperatures.

Table 1: Results after burning samples

Samples	Mass after burning (g)	Compressive Strength (kgf/cm^2)
Remained of delivery	**"green": 8 ,00**	**2,2/3,14 = 0,7 kgf/cm^2**
1 – 400ºC	**8,00**	**9/3,14 = 2,86 kgf/cm^2**
2 – 400ºC	**7,90**	**12/3,14 = 3,82 kgf/cm^2**
3 – 400ºC	**8,00**	**20/3,14 = 6,3 kgf/cm^2**
4 – 600ºC	**7,90**	**25/3,14 = 7,96 kgf/cm^2**
5 – 600ºC	**7,80**	**25/3,14 = 7,96 kgf/cm^2**
6 – 600ºC	**8,00**	**26/3,14 = 8,28 kgf/cm^2**
7 – 800ºC	**7,70**	**283/3,14 = 90,12 kgf/cm^2**
8 –800ºC	**7,70**	**310/3,14 = 98,72 kgf/cm^2**
9 – 800ºC	**7,50**	**325/3,14 = 103,50 kgf/cm^2**
10 – 1000ºC	**7,50**	**1200/3,14 = 382,16 kgf/cm^2**
11 – 1000ºC	**7,40**	**1570/3,14 = 500,00 kgf/cm^2**
12 – 1000ºC	**7,60**	**1325/3,14 = 421,97 kgf/cm^2**

Table 2: Calculation of Porosity and real Density by BET method (Braunau, Emmet and Teller):

Sample	Density	Specific Surface BET	Microporosity	Área of micropores	Average size of micropores	Total pore volumes	Maximum diameter	Average diameter
	(g/cm^3)	(m^2/g)	(cm^3/kg)	(m^2/g)	(nm)	(cm^3/kg)	(Å)	(Å)
Untreated PPS	2,667	9,046	0,00439	12,430	4,715	0,02450	1328,80	108,40
Treated PPS	2,699	6,034	0,00292	8,273	5,093	0,01841	1293,80	122,10

With this study, we determined that the PPS (powder of soapstone) has a great potential to be added as raw material in the manufacture of refractory, especially as resistance to abrasion and shock (fireplaces, grills, ceramic parts for electrical use, etc.) . Thus, besides the economic point of view of using a waste found in abundance in the state of Minas Gerais, this study proposes a compelling alternative to minimize environmental problems caused by the discharge of dust into nearby rivers and springs, adding value to waste.

Acknowledgments

The authors would like to acknowledge FAPEMIG and CNPq for helping the professor in the research conducted so to CNPq a part of financing the trip to Australia.

Physical Chemistry of Protoplanetary Disks

Francesco C. Pignatale[1], Sarah T. Maddison[1], Geoffrey Brooks[2], Kurt Liffman[3]

[1]Centre for Astrophysics & Supercomputing, Swinburne University
[2]Departments of Mathematics, FEIS, Swinburne University
[3]CSIRO/MSE

Studying protoplanetary disks and their dust content is crucial for understanding the processes leading to the formation of planets. Protoplanetary disks result from the conservation of angular momentum in a collapsing, rotating cloud of gas and dust. Typical dimensions of these disks are of the order of a few 100 AU (1 AU= 149.60 x 10^6 Km) with lifetimes of 1-10 Myr (Henning 2008).

Solar system bodies such as planets, meteorites and comets are all created from solids during the protoplanetary disk phase. The physical conditions in the disk, like temperature, pressure, density, heating and cooling processes, together with dynamical processes such as turbulence, radial mixing, inward accretion and outward jet flows, determine a wide range of thermodynamic conditions in which the first grains condense out of the gas phase. The processes of grain formation are then intrinsically related to the chemistry of the disk. Indeed, the materials that form in the disks are a mixture of condensates with different chemical compositions and properties, reflecting the wide range of physical conditions in the disk (Henning & Meeus 2009).

The quantity and quality of observations of disks around young stars has increased in recent years: the Spitzer space telescope and the new Herschel space telescope have provided a large amount of useful data at infrared wavelengths, whose interpretation provides information on the composition, growth and thermal processing of dust grains in the disk (Olofsson et al. 2009). Together with these observations, the study of objects in our solar system provides direct and accessible evidence of the chemistry of the young solar system and the thermodynamic condition in which they formed. Meteorites, among the oldest object in our solar system (4.5 Gyr), are characterized by heterogeneous compositions and show a mixture of compounds that are the results of condensation processes in different environments and evolutionary phases of the disk (Scott 2007). Even comets show this heterogeneity indicating complex thermodynamic and dynamic scenarios. Comets contain a mix of particles that must have formed in the inner region of the solar system and experienced high temperature processes, next to other material clearly produced by cold thermodynamic environment (Zolensky et al. 2006). Observations of these solar system bodies suggest that the temperature in the disk ranged from 2000 K to 20 K and the pressure from 10^{-2} to 10^{-10} bar.

Further clues about the chemical composition can be inferred by the solar photosphere composition: hydrogen, oxygen, carbon, nitrogen, magnesium, silicon and iron are the most abundant elements in the solar photosphere and all the object in the solar system are constituted by their compounds.

A widely used approach in the modeling of the behaviour of gas-dust systems in protoplanetary disks is assuming thermodynamic equilibrium of the system within a wide range of disk models. Even if the disks are not in total equilibrium, the time scale of the

protoplanetary disk phase can overcome the kinetics barrier, mass transfer, reaction rates and surface phenomena allowing the system to reach an equilibrium state. The use of the Gibbs free energy minimization technique, together with the study of the condensation sequence, allows astronomers to predict the chemical composition in different zones of protoplanetary disks at different conditions.

Molecular hydrogen, water vapor, CO and CH_4 are the main gases in protoplanetary disk (for a solar composition system), while silicates, like enstatite and forsterite, and ice are the most abundant solids. However, the initial composition of the system can change dramatically the final products of condensation and hence extrasolar planetary systems are expected to differ from those in our solar system. To date 500 planets have been discovered around different stars but as yet no Earth-like analogues have been found.

Many studies in the past made the common assumption of an ideal solution describing the behaviour of compounds in the system. This approach is good enough to return a general chemical distribution within the protoplanetary disk as observed. However it does not take in account other important parameters involved in chemical reactions like the temperature and the composition.

In this talk we present an overview of the physical properties of protoplanetary disks, the chemistry of the main objects of our Solar System and our advance in modeling by the incorporation of the regular solution model in the computation of the gas distribution and the condensation sequence of solids within the disk.

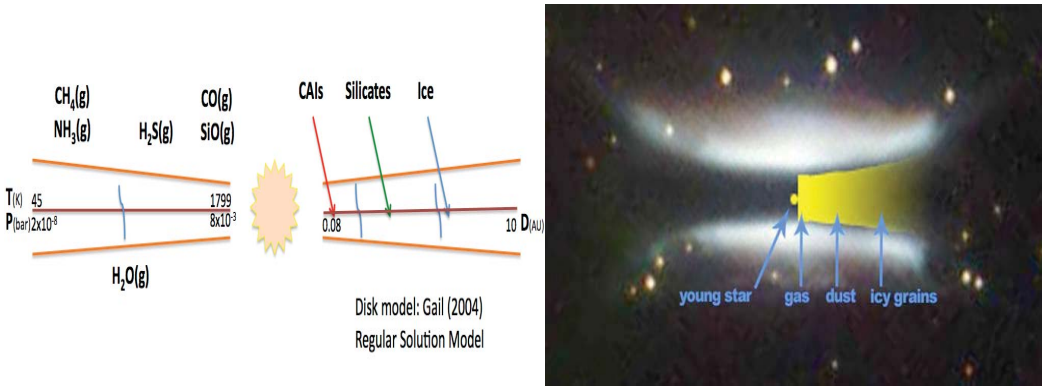

(Left) Gas and solids distribution in a midplane of protoplanetary disk calculated using the regular solution model. Physical conditions (T and P) are taken from the disk model of Gail (2004). (Right) IRAS 18059-3211 from Hubble Space Telescope. This object is an edge-on disk in which thick dust obscures the young central star. The starlight is scattered off the less dense upper layers of the disk producing a butterfly-like morphology.

(www.stsci.edu)
Gail H., 2004, A&A, 378,192;
Henning T., 2008, Phys. Scr., T130, 014019;
Henning T., Meeus G., 2009, preprint, abs/2009arXiv0911.1010H;
Olofsson J., Augereau J., van Dishoeck E. F., et al., 2009, A&A, 507, 327
Scott E., 2007, Annual Review of Earth and Planetary Sciences, 35, 577;
Zolensky et al., 2006, Science, 314, 1734

Processing, Characterisation and Mechanical Properties of Metal Foams

Cuie Wen
IRIS, Faculty of Engineering and Industrial Sciences, Swinburne University of Technology
Hawthorn, Victoria 3122, Australia

Key words: metal foams, mechanical properties, powder metallurgy, sintering

Metal foams and other highly porous metal materials exhibit unique combinations of excellent mechanical, thermal, electrical and acoustic properties that provide opportunities for a wide range of applications. The recent development of a number of cost-effective processes for making metal foams has increased their potential for applications in biomaterials, sandwich panels for lightweight structural components, in energy absorption devices for protection from impact, in heat sinks for electronic devices and in noise attenuation etc.

Porous titanium and titanium alloys have been developed for orthopaedic and dental applications in recent years.[1,2] This new class of metal scaffolds are receiving increasing attention due to their excellent biocompatibility, bone-mimicking architecture and mechanical properties which ensure new bone tissue ingrowth ability, vascularisations and eliminating stress shielding effect. Porous titanium and titanium alloy foams can be conveniently produced by powder metallurgy. A Ti6Ta4Sn alloy scaffold fabricated by powder metallurgy with osteoblast-like cells growing into the porous structure is shown in Figure 1.[3]

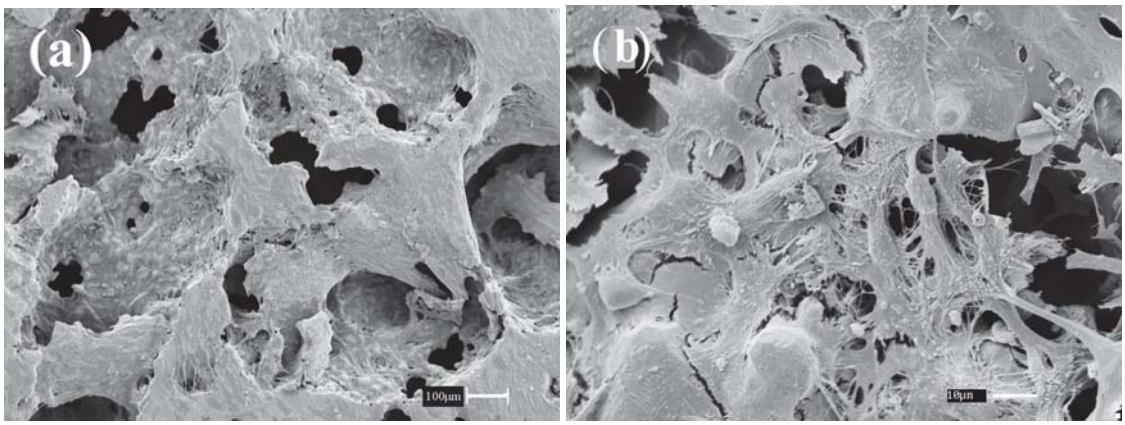

Figure 1. Scanning electron microscopy images showing $SaOS_2$ cells attachment on porous Ti6Ta4Sn disc (a) and high magnification image (b).[3]

Aluminium, magnesium and their alloy foams have been developed for automotive, personal protection (e. g. armour), and construction applications etc.[4] Several cost-effective processing methods have been developed for manufacturing aluminium, magnesium, and their alloy foams including both powder metallurgy and liquid processing in the last decade. The foaming mechanism, characterisation, mechanical and physical properties have been investigated extensively. This new class of metal foams are ultra-light, possessing high energy absorption capacity and damping ability, as well as various functionalities. One typical application of the aluminium alloy foams can be find in the sandwich panels for automobile parts and the use of metals foams can make the cars safer, stronger and more

comfortable. Figure 2 shows the different deformation modes under compression of an aluminium tube with and without a foam filling. The foam filled tubular structure shows a significant enhancement of energy absorption under compression.

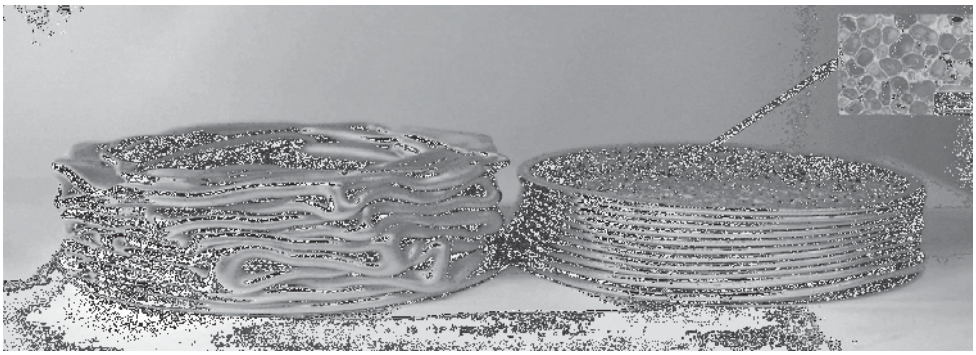

Figure 2. Photographs of the axially crushed empty tube and the foam filled tube.

Among lightweight metal foams, nickel foams are also highly interested since they can be used as electrodes of nickel cadmium and nickel metal hydride batteries for electric vehicles, catalysts, diesel particulate filters, silencers and so on.[5)] Nickel foams can be produced by metal deposition on polyurethane foams and powder metallurgy.

The present review examines the current information on the processing, characterisation, mechanical properties and potential applications of different kinds of metals foams. This paper will include the three main aspects: (i) microstructural features, mechanical and functional properties of metal foams; (ii) main processing methods for manufacturing metal foams; (iii) typical examples of titanium, aluminium, magnesium and nickel foams.

References

1. C. E. Wen, M. Mabuchi, Y. Yamada, K. Shimojima, Y. Chino and T. Asahina (2001), "Processing of biocompatible porous Ti and Mg", *Scripta Mater.*, Vol.45, No.10, pp. 1147-1153.
2. C. E. Wen, J. Xiong, Y. Li, P. D. Hodgson, "Porous Shape Memory Alloy Scaffolds for Biomedical Applications: A Review", *Physica Scripta*, T139, 2010, pp. 014070
3. Y. C. Li, J. Y. Xiong, C. S. Wong, P. D. Hodgson, C. E. Wen, "Ti6Ta4Sn Alloy and Subsequent Scaffolding for Bone Tissue Engineering," *Tissue Eng.*, Vol.15, No.10, 2009, pp. 3151-9.
4. Y. C. Li, J. Y. Xiong, J. G. Lin, M. Forrest, P. D. Hodgson and C. E Wen, "Mechanical Properties and Energy Absorption of Ceramic Particulate and Resin-Impregnation Reinforced Aluminum Foams", *Materials Forum*, Vol.31, 2007, pp. 53-56.
5. Y. Yamada, Y. C. Li, T. Banno, Z. K. Xie and C. E. Wen, "Micro-porous Nickel Produced by Powder Metallurgy", *Mater. Sci. Forum,* Vol.534-536, 2007, pp. 977-980.

Revision of Quasi-chemical Viscosity Model to Predict Viscosity of Molten Slag in Multicomponent Oxide Systems related to Metallurgical Processes

Masanori Suzuki, Evgueni Jak
Pyrometallurgy Research Centre, School of Chemical Engineering,
The University of Queensland, St Lucia, Brisbane, QLD 4072 Australia

Key words: slag viscosity, viscosity modelling, fully liquid slag, viscous flow structural unit, multicomponent oxide systems

Knowledge on viscosity of molten oxide slag has been of a significant importance in various kinds of metallurgical processes for metal production. Viscosity of molten slag is related to internal structure of oxide melt, and very sensitive to the changes of temperature and slag composition. Generally, slag viscosity has difficulty in being precisely measured, and predicted by empirical methods. Therefore, the development of a reliable viscosity model has been required to accurately and reasonably estimate slag viscosities over whole composition range for multicomponent oxide systems through the structural features of oxide melts.

For the precise estimation of slag viscosities, the authors have been revising the quasi-chemical viscosity (QCV) model that had been previously developed for multi- component silicate systems. [1)] This viscosity model enables viscosity of molten slag at a given temperature and composition to be predicted through the oxygen anions associated with various kinds of cations, which are referred to as the viscous flow structural units. The concentrations of the structural units in oxide melt are derived from the Gibbs energy minimizing calculation for the liquid phase based on the quasi-chemical thermodynamic model. [2)] Therefore, the QCV model proposes a link between viscosity and thermodynamic properties of molten slag.

Although the previous QCV model reproduced experimental viscosity data in the limited composition range, a model revision has been required to reproduce the significant viscosity change at high SiO_2 concentrations and the composition dependence of slag viscosities in non-silicate aluminate systems. In this study, the revision of the quasi-chemical viscosity model formalism has been performed to accurately estimate viscosity of molten slag over wide composition ranges for various oxide systems including high SiO_2 concentration ranges and aluminate systems.

The quasi-chemical viscosity model is derived by applying the following Eyring equation to describe the viscosity of a liquid to oxide melts:

$$\eta = \frac{2RT}{\Delta E_V} \frac{(2\pi m_{SU} kT)^{1/2}}{v_{SU}^{2/3}} \exp\left(\frac{E_a}{RT}\right) \quad (1)$$

where R and k are the gas and Boltzmann constants respectively, and T is the absolute temperature. m_{SU} and v_{SU} represent the average mass and volume of a viscous flow structural unit in the system. The activation energy, as described by E_a in Equation (1), corresponds to the potential barrier for a structural unit to jump over, and it reflects the interactions between

different structural units in the liquid. The vaporization energy ΔE_V is related to the energy of hole formation, which determines the concentration of hole in the liquid.

It is assumed that molten slag consists of nearly close-packed arrangement of oxygen anions with associated cations. To apply the above Eyring viscosity equation to slag viscosities in oxide systems, the authors define the structural units in oxide melt as the oxygen anions associated with various kinds of cations. For instance, the SiO_2-MeO binary silicate slag consists of three types of structural units: (Si-O-Si), (Si-O-Me) and (Me-O-Me). Then, we assume that the average mass and volume of a structural unit, the integral activation energy and vaporization energy are expressed as functions of the concentrations of these structural units in the melt.

In the QCV model, the calculated result of slag viscosity depends on the formalism of the activation and vaporization energies as major model coefficients. In this study, their mathematical formalism for binary silicate systems has been revised using a power function of the (Si-O-Si) and (Si-O-Me) structural units with system-dependent coefficients. This power function expresses attractive interactions between the oxygen anions in the (Si-O-Si) structural units and basic cations in the (Si-O-Me) structural units, and they are assumed to result in the significant decrease of viscosity at high SiO_2 contents by the addition of basic oxides into the system. The steepness of the viscosity change has been dependent of the geometric and electronic properties of basic cation.

Figure 1 shows the calculated results of slag viscosity in the SiO_2-CaO system. The predicted viscosities by the present model show much more extreme changes at high SiO_2 concentrations than those by the previous model, and they strictly reproduce all available experimental results. Therefore, it is found that the revised QCV model is able to accurately reproduce the composition dependence of viscosity over the whole composition range, including high SiO_2 concentration range in binary silicate systems. The revised model formalism has been applied for various binary silicate systems including SiO_2-Al_2O_3, SiO_2-MgO and SiO_2-Na_2O, and good agreements have been obtained between the predicted and experimental viscosities of molten slag.

In Al_2O_3-containing systems, it has been revealed that Al^{3+} cations form tetrahedral coordination instead of octahedral as a result of charge compensation by basic cations, and the presence of tetrahedral Al^{3+} can enhance viscosity of the oxide melt due to the formation of strong covalent bond with neighbouring oxygen anions. Although tetrahedral Al^{3+} can exist in the structural units containing Al^{3+} cations, the quasi-chemical thermodynamic model cannot distinguish tetrahedral and octahedral Al^{3+} as the concentrations of structural units are derived. In this study, the proportion of tetrahedral Al^{3+} in total amount of a given Al^{3+}-containing structural unit has been mathematically identified. The contributions of tetrahedral and octahedral Al^{3+} on slag viscosities have been individually evaluated in the activation and vaporization energy formalisms for binary aluminate and ternary aluminosilicate systems.

The revised QCV model formalism has been successfully extended to multi- component oxide systems, and slag viscosities has been critically evaluated with the same set of model coefficients as determined for binary and ternary systems. The accuracies have been improved from the previous QCV model to reproduce all reliable experimental viscosity data over wide temperature and composition ranges.

In addition, viscous behaviour of molten slag has been predicted using the revised QCV model for the composition range of interest to metallurgical processes where no experimental results are available. **Figure 2** shows the predicted iso-viscosity contours of molten Al_2O_3-CaO-MgO-15 mass% SiO_2 system at 1873 K, which can include ladle slag compositions formed in BOF or EAF process in iron and steelmaking. The sum of mass fractions of all components except SiO_2 has been converted into unity.

In conclusion, the quasi-chemical viscosity model formalism has been revised so that viscosities of molten slag can be accurately predicted over wide composition ranges for various silicate systems including high SiO_2 concentration ranges, and non-silicate aluminate systems.

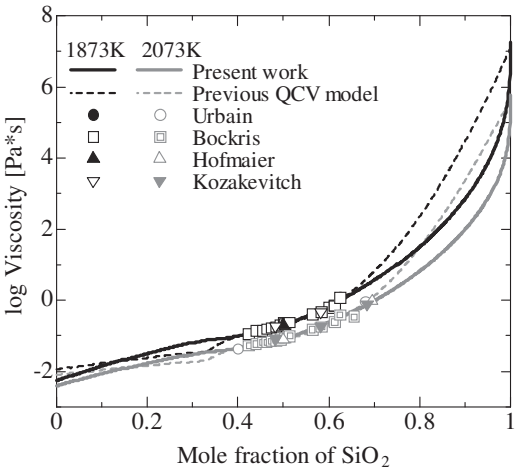

Figure 1. Calculated viscosity of molten slag in the SiO_2-CaO system.

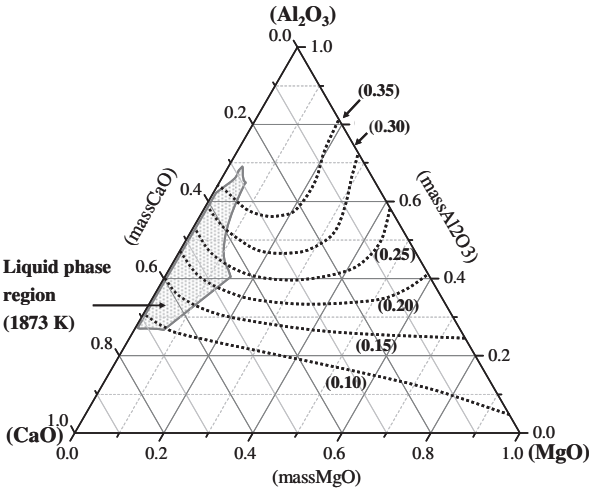

Figure 2. Calculated iso-viscosity contours in the Al_2O_3-CaO-MgO-15 mass% SiO_2 system at 1873 K. (Viscosity: Pa*s)

References

1. A.Kondratiev and E.Jak, "A Quasi-Chemical Viscosity Model for Fully Liquid Slags in the Al_2O_3-CaO-'FeO'-SiO_2 System," *Metall. Mater. Trans.*, Vol. 36B, 2005, pp. 623-638.
2. A.D.Pelton and M.Blander, "Thermodynamic Analysis of Ordered Liquid Solution by a Modified Quasichemical Approach – Application to Silicate Slags," *Metall. Trans.*, Vol. 17B, 1986, pp. 805-815.

Five Key Challenges Facing Pyrometallurgy

Professor Geoffrey Brooks

Swinburne University of Technology
FEIS, Hawthorn, 3122 Australia
email: gbrooks@swin.edu.au

Pyrometallurgy is a mature field of human knowledge, which has played a key role of the development of modern technological society. In the 20th Century, pyrometallurgy under went several scientific and technological revolutions, of particular importance was, the widespread introduction of large scale continuous processing, greater process intensity and productivity through developments in gas injection technology, the development of recycling technologies for mass production of high quality products, the development of a rigorous physical chemical description of processes and the introduction of computers in data collection, data analysis, process control and modelling. In the later half of the century, there was increased emphasis on environmental controls and lowering the ecological impact of the various processes, which, in turn stimulated various developments in process design and control. By in large, these developments lead to significant improvements in energy efficiency, productivity, product quality and the lowering of emissions.

The achievements aside, significant problems still face pyrometallurgy as a field. In fact, some challenges have magnified, as metal production continues to grow (particularly, in China) but there also increased social pressure to lower the ecological footprint of metal production. Of course, technological issues are linked to fundamental scientific challenges, and to scientific advances outside the field of pyrometallurgy. In the Western world, these challenges must be addressed in an environment where there has been a clear shift in scientific research and education towards biological and biochemical systems, away from more "traditional" areas of knowledge like pyrometallurgy.

The author has identified five specific challenges that he judges to be very important. Of course, these choices are debatable and open to much criticism but these are presented for that purpose i.e. to promote debate and discussion. They are, in turn:

1) Development of a sustainable high temperature process routes for light metals

2) On line analysis of molten phases

3) Computational kinetics for design and control

4) Continuous steelmaking

5) Attracting the best minds

An analysis of these issues and some ideas on how they can be addressed will be presented by the author.

The Dark Side of Light Metals: Dealing with Oxidation and Dross

John A. Taylor

CAST Cooperative Research Centre (CAST CRC), School of Mechanical & Mining Engineering
University of Queensland, Brisbane, QLD 4074, Australia

Aluminium loves to exist as an oxide, Al_2O_3 [1]. This oxide was probably the first refractory phase to condense from the early solar nebulae [1]. Rubies and sapphires (Al_2O_3, corundum) are hard and stable naturally-occurring precious minerals. Bauxite (an impure hydrated form of Al_2O_3) needs to be coerced, at the expense of 125-210 GJ energy usage and 10-22.5 t CO_2 emissions through the entire extraction process (in particular, energy production for the Hall-Héroult electrolytic refining stage), into the final form of a 1 tonne bundle of purity Al ingot ex. smelter [2]. Aluminium is therefore quaintly (and often disparagingly) referred to as "solidified electricity", implying the need to be extremely cautious with its use since it is one of the most energy-intensive engineering materials. Fortunately, aluminium alloys have also had good press, being highly versatile and durable in service and being readily recyclable (at about 5% of the energy required to produce the primary Al initially). However, the ground is shifting and with the growing focus on embodied energy and carbon footprints, aluminium's processing and use is being revisited.

The general rule in nature is; the more energy it requires for a reaction to take place, the more likely it is that the reaction will try to reverse itself. In the case of aluminium, if there is any oxygen around, it will try and re-combine with it, rapidly, in the order of milliseconds. The big question is: why doesn't aluminium just completely oxidise away? Instead, it seems very stable. The answer is; it would, except that the oxide skin on solid Al, and to a lesser extent, the initial skin that forms on molten Al is highly protective against further oxidation once the initial burst of rapid oxide formation occurs [3]. However, oxide films on molten Al surfaces are easily fractured when subjected to stresses during liquid disturbances, e.g. pouring, splashing, in smelter cast houses and foundries. This leads to further oxidation of fresh metal.

During production of Al products in the smelter cast house, a net metal loss of around 1% of total throughput typically arises from the normal handling, alloying and treatment of the melt via re-oxidation and dross formation. For an overview of this and also more detail on the oxidation process, see Taylor [4].

With a worldwide annual production of some 25 Mt of primary Al, a typical 1% net melt loss (i.e. after metal recovery from dross) amounts to a net loss of 250,000 t/a of saleable metal. At US$ 2000/t for purity ingot, this is effectively US$ 500 million of lost revenue at the expense of some 55 x 10^6 GJ of wasted energy and 3.0 - 5.75 Mt of unnecessary CO_2 emissions every year [2]. In today's energy- and environmentally-conscious world, the drive for increased fuel efficiency and light-weighting in the transport sector surely needs to be matched by a similar drive to reduce the currently-accepted typical metal losses from the cast

[1] From thermodynamics alone, the formation of Al_2O_3 on a fresh liquid Al surface at 750°C occurs spontaneously if the partial pressure of oxygen, $P_{O2} > 10^{-43}$ - 10^{-38} kPa [7]. These are exceptionally low pressures found in the vacuum of deep space, not in aluminium furnaces. The ΔG^o_f for the reaction $4/3[Al] + O_2 = 2/3<Al_2O_3>$ is -900.86 kJ ± 16.74 kJ at 750°C [8].

house. Clearly, even small gains in reducing melt loss by tackling oxidation and dross formation are worthwhile.

The issue of dross reduction has been on the agenda of cast houses for many years now but it remains a poor cousin to the reduction, carbon and casting processes and therefore progress has been generally slow. Since 1986, Van Linden [5] has advocated a rigorous procedure to analyse at which stages in the production cycle (i.e. equipment/process step) that dross is produced and what metal content that dross contains. In this way, the major culprits for metal loss can be identified and addressed. In his opinion, cascade pouring is "the second highest skim volume generator" after remelt of Mg-containing Al alloy scrap.

Clark and McGlade [6] conducted a survey in 2005 of the Australian/New Zealand primary Al smelters and found that among cast house practitioners it was generally accepted that 80% of cast house melt losses occur in the casting furnace, and 60% of those are generated during furnace filling, typically "cascading" events (Fig. 1). If we consider, a furnace of 50 t primary Al and assume a typical 1% net metal loss formed during processing (i.e. 500 kg), then according to their data, 240 kg metal loss (48%) would result directly from the furnace filling activity. Assuming all dross arises from full conversion of liquid Al to oxide (an over-estimate), then this would lead to a net weight gain of 213 kg due to oxygen uptake. For smaller test amounts, this should be measureable, e.g. controlled pours of 100 kg should result in up to 420g gains.

Research into the oxidation of molten aluminium and its alloys appears to have begun in earnest in the early 1960s with Radin [9] and Thiele [3]. It has remained of topic of interest ever since with many works published in the field, in particular, experimental studies based on thermogravimetry and microstructural forensic analysis of oxide films, e.g. [7], with only a few that explore other approaches, e.g. [10]. Oxidation mechanisms, especially the various stages, have been well described qualitatively, yet there has to date been no quantitative oxidation rate model generated that can be used to predict the amounts of oxide (and hence dross) that might occur during normal industrial melt handling scenarios.

CAST has a particular interest in being able to numerically model and simulate the oxidation of aluminium and dross formation at an industrial scale so that potential solutions (equipment and/or process) can be modelled prior to costly plant introduction. It has adopted several research approaches to achieve this.

Firstly, we use an experimental skimming technique (Fig.1) described by Freti *et al.* [10] in 1982 in order to develop usable oxidation rate algorithms. These tests operate across the time scale from ~15 secs to several hours. It was found that the overall oxidation rate (OOR) at ~800°C (750-850°C range) is governed by a power law relationship of the form, $OOR = a \cdot t^b$ (g m^{-2} s^{-1}) where t is holding time (seconds) and a, b are fitting constants. Secondly, we are exploring oxidation at very small times scales, e.g. 1 ms, using a laser ablation technique with fast image capture and analysis. Thirdly, we have conducted medium-scale cascade pouring experiments with up to 350 kg melt transfers with fall heights up to 920 mm (Fig. 2) from which oxide weight gains were determined and which could then be compared with SPH modelling simulation results using the same experimental conditions and the developed oxidation rate model.

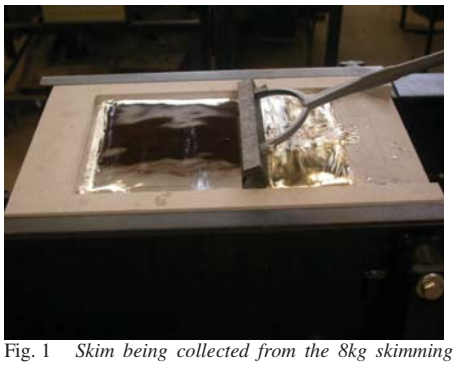

Fig. 1 *Skim being collected from the 8kg skimming rig using a scraper blade.*

Fig. 2 *500 kg tilting furnace and slung sow mould used for medium-scale pouring experiments.*

These approaches are providing useful insights that appear to contradict oxidation expectations based on industrial anecdotes. Rather than supporting the current view that turbulent melt pouring events generate large amounts of oxide in the time-scale of the pour, it appears that only small physical amounts of oxide are actually formed, but that these may predispose melts in industrial furnaces to generate large amounts of dross subsequently by other yet undescribed means. CAST hopes to unravel this in the future and so positively impact the drive to reduce energy wastage and CO_2 footprint issues arising from re-oxidation.

References

1. T.R. Ireland, B. Fegley, Int. Geological Review, 2000, 42, 865-894.
2. T.E. Norgate, S. Jahanshahi, J. Rankin, Journal of Cleaner Production, 2007, 15, 838-848.
3. W. Thiele, Aluminium, 1962, 38 (11, 12), 707-715, 780-786.
4. J.A Taylor, Proc. 10th Australasian Conf. Alum. Cast House Technol., Sydney, 6-9 Aug 2007, 47-55.
5. J.H.L. Van Linden, Light Metals 1986, (Warrendale, PA: TMS, 1986), 785-792.
6. A. Clark, P. McGlade, 3rd International Melt Quality Workshop, Dubai, UAE, 14-16 Nov 2005, 8 pp.
7. S.A. Impey, PhD thesis, 1989, Cranfield Institute of Technology, 243 pp.
8. San José State University, http://www.engr.sjsu.edu/ellingham/ellingham_tool_p1.php
9. A.Y. Radin, Trudy. Moskov. Aviatsion. Tekhnol. Inst., 1961, 49, 73-97.
10. S. Freti, J.D. Bornand, K. Buxmann, Light Metals 1982, (Warrendale, PA: TMS, 1986), 1003-1016.

Grain Size in Cast Light Metal Alloys: The Interdependence Model

Mark Easton[1,3], Ma Qian[2,4], David StJohn[1,4]

[1]CAST Co-operative Research Centre
[2]ARC Centre of Excellence for Design in Light Metals
[3]Department of Materials Engineering, Monash University, Vic 3800,
[4]School of Mechanical and Mining Engineering, The University of Queensland, Qld 4072

Keywords: grain refinement, solidification, nucleation, aluminium, magnesium

Grain refinement during solidification improves alloy properties, reduces defects such as hot tearing and porosity and leads to a more homogeneous product for improved processing. Controlling the grain size of a casting is therefore of great importance. The grain size, d, has been found to be related to the composition of an alloy [1] via the inverse of the growth restriction factor Q via a simple relationship

$$d = a + b/Q \quad (1)$$

where $Q = m_l c_0 (k-1)$, where m_l is the gradient of the liquidus, C_o the alloy composition, and k the partition coefficient. It has been shown that experimental data for a number of alloy systems fit the linear form of Eq. (1) [2-11]. a was observed to be related to the nucleant density and b to the nucleant potency [1].

More recently, the authors have developed a rigorous physical basis for the model The grain size of a casting is shown to be dependent upon the distribution of nuclei, the amount of growth before nucleation in the constitutionally supercooled (CS) zone, and the size of the CS zone, and consequently the interdependence of grain nucleation and growth (Fig. 1a), i.e.

$$d = r_{cs} + r_{dl} + r_i \quad (2)$$

The first measure is the distance, r_{cs}, the previous grain must grow to generate sufficient constitutional supercooling ΔT_{cs} that can trigger nucleation on a particle of potency ΔT_n (i.e. requiring $\Delta T_{cs} \geq \Delta T_n$). A consideration of both spherical and planar growth has shown that r_{cs} is equal to $D\Delta T_n/vQ$ [12], where D is the diffusion coefficient and v is the growth velocity.

The second distance, r_{dl}, is the diffusion length from the S-L interface, r_{cs}, of the previously nucleated grain to where ΔT_{cs} is at its maximum value. Consideration of growth of the solid and the diffusion boundary layer in the initial transient has indicated that r_{dl} is defined [13] by

$\frac{4.6 \cdot D}{v} \cdot \left(\frac{C_l^* - C_0}{C_l^* \cdot (1-k)} \right)$, where C_l^* is the composition of the liquid at the interface.

Given that r_i has been previously shown to be related to the inverse cube root of the nucleant particle density [1], , a physically based equation for grain size can be expressed as

$$d = \frac{D\Delta T_n}{vQ} + \frac{4.6 \cdot D}{v} \cdot \left(\frac{C_l^* - C_0}{C_l^* \cdot (1-k)} \right) + \frac{1}{\sqrt[3]{fN_v}} \qquad (3)$$

where N_v is the number of nucleant particles added, and f is the proportion that are active. This relationship and is expressed graphically in Fig 1(b). Interestingly, r_{cs} + r_{dl} represent a 'nucleation free zone' that is a practical lower limit on the amount of grain refinement achievable.

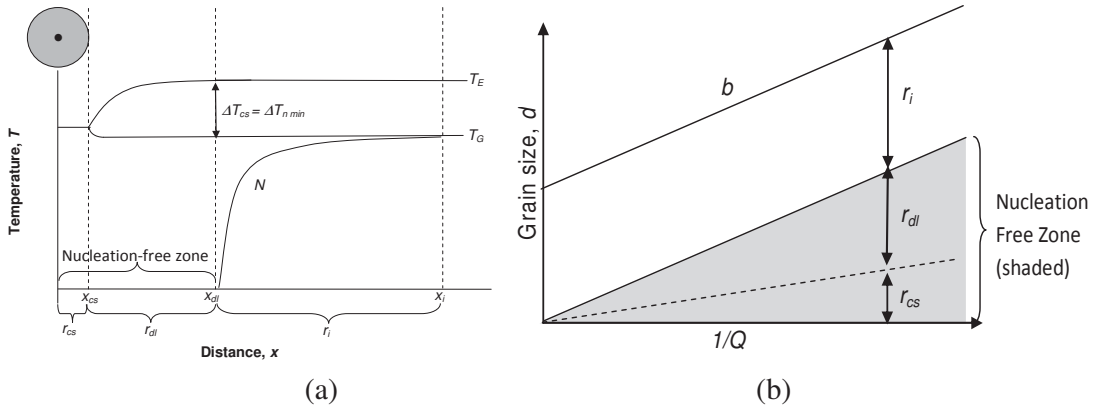

Figure 1. (a) A schematic showing the three regions that together establish the grain size of the microstructure: r_{cs}, r_{dl} and r_i. r_{cs} and r_{dl} together represent a nucleation-free zone where nucleation is not possible for the potency and spatial distribution of the particles described by *N*. (b) A simple representation illustrating that for each value of *Q* the grain size is the result of three components: r_i is the average distance between activated particles and *b* is equal to the gradient of r_{cs} plus r_{dl} over a unit of *1/Q*. The shaded area is the nucleation-free zone and represents the minimum grain size that can be achieved for each value of *Q*.

References

1. M.A. Easton and D.H. StJohn: *Metall. Mater. Trans. A*, 2005. vol. 36A(7), pp. 1911-1920.
2. A.V. Nagasekhar, M.A. Easton, and C.H. Cáceres: *Adv. Engng. Mater.*, 2009. vol. 11(11), pp. 912-919.
3. A. Becerra and M.O. Pekguleryuz: *Journal of Materials Research*, 2009. vol. 24(5), pp. 1722-1729.
4. T.V. Atamaneko, D.G. Eskin, L. Zhang, and L. Katgerman: *Metall. Mater. Trans. A*, 2010. vol. 41A(8), pp. 2056-2066.
5. M.J. Bermingham, S.D. McDonald, M.S. Dargusch, and D.H. StJohn: *Scripta Mater.*, 2008. vol. 58, pp. 1050-1053.
6. M.J. Bermingham, S.D. McDonald, K. Nogita, D.H. StJohn, and M.S. Dargusch: *Scripta Mater.*, 2008. vol. 59, pp. 538-541.
7. D.H. StJohn, M. Qian, M.A. Easton, P. Cao, and Z. Hildebrand: *Metall. Mater. Trans. A*, 2005. vol. 36A(7), pp. 1669-1679.
8. D.H. StJohn, M.A. Easton, and M. Qian: *Solid State Phenom.*, 2008. vol. 141-143, pp. 355-360.
9. M. Qian and A. Ramirez: *J. Appl. Phys.*, 2009. vol. 105, pp. 013538.
10. D.H. StJohn, P. Cao, M. Qian, and M.A. Easton: *Adv. Engng. Mater.*, 2007. vol. 9(9), pp. 739-746.
11. A. Ramirez, M. Qian, B. Davis, and T. Wilks: *Int. J. Cast Met. Res.*, 2009. vol. 22 pp. 260-263.
12. M. Qian, P. Cao, M.A. Easton, S.D. McDonnald, and D.H. StJohn: *Acta Mater.*, 2010. vol. 58, pp. 3262-3270.
13. D.H. StJohn, M. Qian, M.A. Easton, and P. Cao: *submitted to Acta Materialia*, 2011.

Case Studies in Application of Mathematical Modelling to Magnesium Direct Chill Continuous Casting

John F. Grandfield[1]
[1]Grandfield Technology Pty Ltd, Brunswick, Victoria, Australia

Keywords: direct chill casting, magnesium, mathematical modelling

Three case studies in application of mathematical modelling to solving problems in direct chill casting of magnesium are reviewed and lessons learnt revealed.

The three case studies are;

i) Shell tearing causing liquid breakouts during horizontal direct chill casting pure Mg and AZ91 (1,2)
ii) Centre hot tearing & surface tearing at cast start for AZ31 vertical DC casting of extrusion billet (3) and
iii) Cold cracking during DC casting of high strength WE43 slab (4).

From 1996 through 2000 an attempt was made to develop HDC casting technology to produce magnesium small remelt ingots in the same manner as the aluminium industry. One of the key determinants of the cost of production of HDC casting is the length of continuous run time. In the case of magnesium this was limited by the incidence of the shell tearing during casting, resulting in liquid break outs and cast aborts. There were also quality problems with the cast bar i.e. centreline cracks. These defects and their formation was examined in detail as part of a PhD (1) which included measurement of mould and shell temperatures, liquid pool doping, FEM thermal modelling and cellular automata finite element grain structure (CAFE) modelling.

The modelling results supported the development of mechanistic explanations of the defect formation, i.e. the low volumetric heat capacity of magnesium and the high thermal conductivity of the refractories used promotes freezing of material onto the refractory and subsequent shell tearing. Additionally, the large columnar grain structure (due to lack of a grain refining agent) promotes centreline cracking requiring slow casting speeds which in turn leads to increase incidence of shell tearing. However, solutions to these problems were not found at the time.

In the second case study a VDC gas pressurised hot top mould technology was developed and applied in a two strand casting unit for 8 inch billets in 2006. The technology was applied to a variety of alloys including AZ31. Extremely high quality surface finish could be obtained as long as fast start conditions were used, however these conditions resulted in centreline cracks. A variety of cast start speed ramp conditions were tested to find the optimum conditions. Later, these conditions were modelled with Alsim(coupled thermal, fluid stress FEA package designed for DC casting simualtion). Prediction of stress and pressure conditions in the semi-solid region where the cracks form was included in this model. The model results correctly coincide with those conditions causing cracks or not (3). The model thus provides a tool for establishing optimum conditions for other alloys.

In the third study (through 2008-2009), the intent was to find casting conditions for WE43 alloy rolling slab such that the slab did not catastrophically crack during or after casting. This type of cracking is a well known problem in the aluminium industry with high strength, low thermal conductivity, low ductility alloys. A full 3D thermal, fluid, stress model was developed using Alsim. Thermocouples were inserted during casting and compared to predictions from the model as was final slab dimensions including rolling face flatness. Extensive thermal and mechanical property measurements were made. It was found that some of the key thermal properties were not as per existing published data. Residual stress measurements and comparison with the model are the subject of a forthcoming 2011 paper. Having verified the model, a sensitivity study was carried out where a wide range of casting conditions were modelled. Note that some of these were of conditions unlikely to be experimentally tested due to safety considerations. Limited experimental trials of different conditions were also made. Examination of the model and experimental results led to formulation of a cracking mechanism and proposed favourable casting conditions. These conditions were tested and crack free product was produced enabling this product to be commercialised.

Major lessons learnt from these projects are;

i) Focus the modelling on the specific problem at hand rather than covering all the process physics i.e. include adequate physics
ii) Ensure you have the correct property and boundary condition data
iii) Experimental verification and testing is absolutely essential but sensitivity studies using models can reduce the amount of physical experiments needed.
iv) Modelling is a necessary but not sufficient ingredient to project success.

References

1. Grandfield, J. F. (2001). Hot tear defect formation during horizontal direct chill casting of magnesium. Brisbane, University of Queensland. PhD.
2. Grandfield J.F. & Dahle A., Modelling and Measurement of Mould Heat Transfer During Horizontal Direct Chill Casting of Magnesium, 4th Pacific Rim International Conference on Modeling of Casting & Solidification Processes, Yonsei, Korea, C.P. Hong et al. eds, Centre for Computer-Aided Materials Processing, Yonsei, Korea, (2000), p299-307
3. J.F. Grandfield, V. Nguyen, & I.F. Bainbridge, Stresses and cracking during direct chill casting of az31 alloy billet, Magnesium Technology 2009, E. Nyberg et al eds, TMS 2009, p129
4. Turski, M, Grandfield J.F., Wilks T., Davis B., DeLorme R., Cho K., ”Computer modeling of DC casting magnesium alloy WE43 rolling slabs”, Magnesium Technology 2010, Agnew, S.R. et al eds, TMS 2010, pp333-338

Thermodynamic Analysis of Transition Metal Borides Formation in Aluminium Melt

A. Khaliq[1,2], M.A. Rhamdhani[1,2], G.A. Brooks[1,2], J. Grandfield[3]
[1]Swinburne University of Technology, Faculty of Engineering and Industrial Sciences, Melbourne, Australia
[2]CAST Cooperative Research Centre (CAST CRC), Australia
[3]Grandfield Technology Pty, Ltd, Brunswick, Victoria, 3055, Australia

Keywords: Transition metals, Thermodynamic analysis, Boron treatment, Borides stability

Smelter grade aluminium can be used as an electrical conductor application if the level of transition metal impurities is controlled precisely.[1] Bauxite and petroleum coke are the main sources of such impurities in aluminium.[2] Most of the impurities have significant effect on aluminium properties.[3, 4] Efforts have been done to supply relatively pure coke to aluminium smelters but still a list of impurities is found in the potline metal.[5-7] The effect of transition metal impurities on electrical conductivity could be minimised if they are out of solution from aluminium and present in some solid phase.[8] Industrially, boron treatment has been employed to combine transition metals into their borides.[9-12] However, solution thermodynamic and reaction mechanism of borides formation are not well understood and further investigations are required. In this article a detailed thermodynamic analysis has been carried out to investigate the formation of borides. It is shown that diborides (MB_2) are the most thermodynamically stable boride compounds of these impurities in the given working conditions. It is also shown that diborides of Zr, Ti, and V are the most thermodynamically stable phases at 650-900^{o}C as compared with Cr and Al diborides. Thermodynamic stability of different phases is also affected by the presence of other diborides phases.

Figure 1 shows the thermodynamic analysis of Al-Zr-Ti-V-Cr-B system having 0.25wt% of each transition metals having 75wt% excess of boron than stoichiometric requirement. It could be observed from Figure 1 that diborides of transitional metals are formed in the given working conditions. Moreover, diborides of Zr, Ti and V are formed preferentially and remained stable but that of Al and Cr dissolve readily as the temperature increased. Due to the excess of boron in the melt, diborides of Al are formed which dissolve at 750^{o}C. after the dissolution of AlB2, the borides of Cr will starts dissolving back into the melt. In the presence of relatively unstable phases i.e AlB_2 and CrB_2, borides of V, Ti and Zr will not dissolve in the given working conditions.

Figure 2 shows the optical microscopic image of Al-V-B systems having 1wt% V and 0.42wt% of B melted and hold for 60 minute at 750^{o}C. It could be observed from Figure 2 that a possible ring of Al,V borides have been formed all around the AlB_{12}. It is further observed that dissolution of AlB_{12} was very sluggish as it remains unmelted even holding the melt at 750^{o}C for 1 hour.

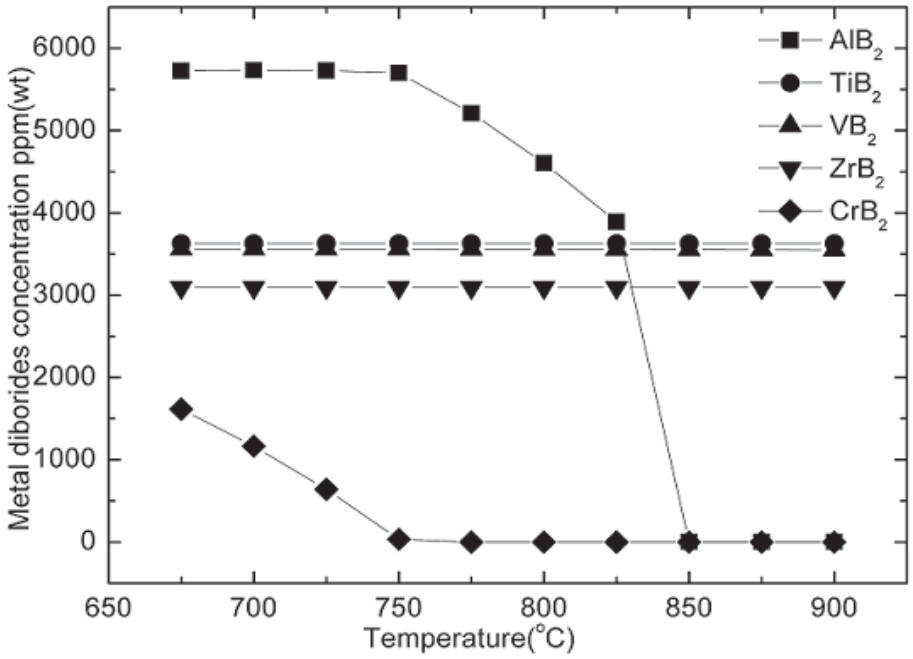

Figure 1: Transition metal borides concentration in Al-Zr-Ti-V-Cr-B system having 75wt% excess boron addition than the stoichiometric requirement.

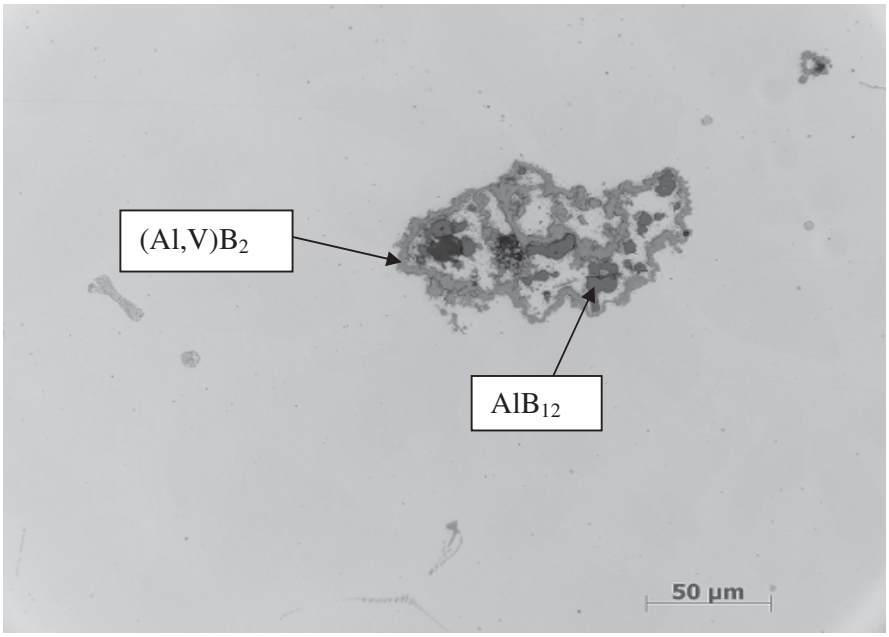

Figure 2: Optical image of Al-1wt%V-0.412wt%B systems melted at 750°C and cooled in air.

References

1. G.G. Gauthier, J. Inst. Met., 59 (1936) 129-150.
2. C.K. K. Grjotheim, M. Malinovsky, K.Matiasovsky, J. Thonstad, Aluminium Electrolysis: Fundamentals of the Hall Heroult Process, 2nd ed., Aluminium-Verlag GmbH, D-4000 Dusseldorf, Germany, 1982.
3. W.A. Dean, Aluminum, 1 (1967) 174.
4. J.F. Grandfield, J.A. Taylor, in: TMS Annual Meeting, 2009, pp. 1007-1011.
5. L.L. McCorriston, in: United States Patent, Gulf Canada Limited, Toronto, Canada, Canada, 1983.
6. P.B. Queneau, in: United States Patent, Amax Inc., Greenwich, Conn., 1984.
7. R. Schemel, in: United States patent, Intevep, S.A., Caracas, Venezuela, Venezuela, 1985.
8. T.A. Engh, Principles of Metal Refining, Oxford University Press, 1992.
9. W. Stiller, T. Ingenlath, Aluminium (English Edition), 60 (1984).
10. W.C. Setzer, G.W. Boone, Light Metals 1992, (1991) 837-844.
11. P.S. Cooper, M.A. Kearns, Aluminium Alloys: Their Physical and Mechanical Properties, Pts 1-3, 217 (1996) 141-146.
12. S. Karabay, I. Uzman, Journal of Materials Processing Technology, 160 (2005) 174-182.

The use of SPH for high temperature processing applications

Mahesh Prakash and Paul W. Cleary

CSIRO Mathematics, Informatics and Statistics
Private Bag 33, VIC 3169, Australia

Key words: Smoothed particle hydrodynamics, flow modelling, oxidation, reaction

In many pyrometallurgical processes pellets or briquettes of raw materials (typically a mix of metal oxide and carbon) are immersed in a hot liquid bath. Heat is transferred to the pellets reducing the metal oxide and forming by products such as gases, metal and slag. This is a complex multi-phase flow with coupled heat transfer and chemical reactions. For many pyrometallurgical processes traditional grid based computational methods, such as the Finite Element Method (FEM) and Finite Volume (or Control Volume methods), produce suitable predictions. However, the inclusion of a large fraction of solids in the liquid metal bath represents significant challenges for these methods.

Liquid aluminum is readily oxidized during melt handling, resulting in the formation of dross (a mix of oxide and trapped metal) that must be skimmed off prior to casting. In a typical primary smelter, the net melt loss is ~1% of total production (a large financial impost and CO_2 footprint), with ~50% estimated to occur during furnace filling. Dross reduction is typically addressed in casthouses by best-guess engineering approaches; however, computational modelling techniques can be used to explore the effects of process design and conditions, thus leading to new strategies for dross minimisation. The main challenge in modelling such flows is the complex free surface and material interface behaviour including fragmentation and splashing. This can often be coupled with complex moving geometry in an industrial melt pouring environment.

Smoothed Particle Hydrodynamics (SPH) [1, 2], a Lagrangian simulation method, is able to simulate both the fluid component including fragmentation and splashing and any immersed solid materials in the fluid. Tracking the motion of the solids, and their interaction with the fluid including both momentum and heat transfer is possible with SPH. Gas generation (for example CO_2) from the solids can be included as well as oxidation of the liquid metal for melt handling applications. The transport of the gas in the bath including the resulting buoyancy effects that may entrain the solids are also able to be simulated [3]. The history dependent nature of the oxide generated during the melt handling process can be represented due to the Lagrangian nature of SPH [4]. Together these allow a good representation of the generation and transport of the solid, liquid and gas components of these complex systems including the important interactions of the gas with the liquid and both the gas and the liquids with any solids.

References

1. P. W. Cleary, M. Prakash, J. Ha, N. Stokes and C. Scott, (2007) "Smoothed particle hydrodynamics: status and future potential", *Progress in Computational Fluid Dynamics*; 7:70-90.
2. J. J. Monaghan, (2005), "Smoothed particle hydrodynamics", *Rep Prog Phys*, 68: 1703-1759.
3. P.W. Cleary, N. Stokes, M. Prakash, J. Ha and G. Brooks, (2005). Simulation of reactive pellets in a pyrometallurgical bath using SPH. *EPD Congress 2005 Edited by Mark E. Schlesinger TMS (The Minerals, Metals & Materials Society)*, 647-654.
4. M. Prakash, P.W. Cleary and J. Grandfield, (2009). Modelling of metal flow and oxidation during furnace emptying using smoothed particle hydrodynamics. *Journal of Materials Processing Technology*, 209, 3396-3407.

Thermodynamic Behaviour of Metallic Impurities in Carbothermal Production of Magnesium Metal

M.W. Nagle, L. Prentice and S. Tassios

CSIRO Process Science and Engineering, Clayton, Victoria, 3168, Australia

Keywords: carbothermal reduction, magnesium

Carbothermal production of magnesium metal has been investigated at CSIRO Process Science and Engineering for a number of years [1,2] and proceeds by the reaction

$$MgO_{(s)} + C_{(s)} = Mg_{(g)} + CO_{(g)} \quad (1)$$

This reaction proceeds at high temperatures in excess of 1400°C, as seen in Figure . However, both the magnesia and carbon are likely to contain various types and amounts of impurities, depending on their source. This work discusses the behaviour of some of these elements based on thermodynamic calculations and attempts to reconcile these with experimental observations.

Figures 1 and 2 show the progress of reactions over a number of hours of heating from room temperature to 1900°C. The pellets are made from fine MgO powder (containing 84.2% MgO, 7.9% SiO_2, 5.5% CaO, 1.0% Fe_2O_3, 0.11% Mn_3O_4, 0.34% Al_2O_3 and 0.12% Na_2O) with a 5% stoichiometric excess of graphite powder.

Progress of the reaction is typically tracked by the evolution of CO as measured by an infrared gas analyser. The CO shows two peaks; one at high temperature associated with magnesium production while the other occurs below 1100°C from the reduction of other metallic oxides. The earlier peak appears greater due to less dilution from nitrogen during subsonic operation.

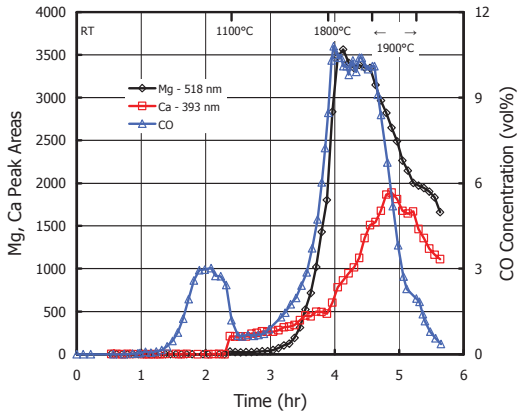

Figure 1: Characteristic area of the peaks for Mg and Ca against elapsed run time compared to CO vol%.

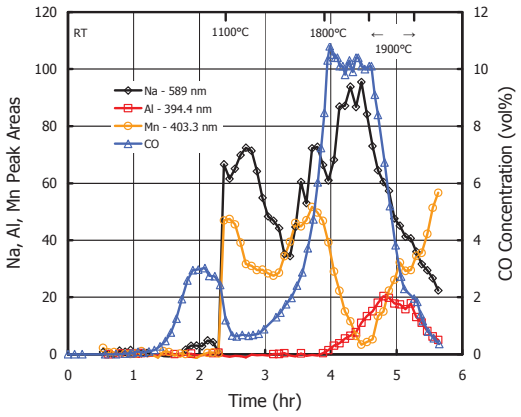

Figure 2: Characteristic area of the peaks for Na, Al and Mn at elapsed run time compared to CO vol%.

CSIRO has recently purchased and commissioned a Laser-Induced Breakdown Spectroscopy (LIBS) analyser for use on the project. This allows us to analyse the stream of gas and solid products passing from the reactor in real time with the ability to directly detect the production of magnesium as well as other elements.

Figure shows that the production of magnesium closely follows the concentration of CO in the gas stream. This is expected as reaction 1 dominates due to the amount of MgO in the system. The concentration of magnesium increases exponentially with temperature, reaches a plateau when the final temperature is reached and then decays as the charge is consumed. However, it should be stressed that the gas composition is far from thermodynamic equilibrium due to kinetic limitations of the carbothermal reaction.

This abstract focuses on the behaviour of a selection of the other elements in the charge and attempts to gain understanding of observed behaviour with the aid of thermodynamic modelling. The behaviour of impurities in the charge have a number of impacts that include the purity of the product metal, the method of removing waste from the reactor, disposal of waste and safe operation of the plant.

The metallic oxides were evaluated individually with a large excess of carbon (to mimic the environment in the reactor) and a nitrogen atmosphere. The calculations were performed using HSC Chemistry Ver. 5.11.

Calcium: Apart from magnesium, CaO tends to be a major impurity in magnesia and calcium is the major metal detected in the gas stream. Given the similarity of the two elements, they would be expected to react in a similar manner and this is borne out by the LIBS analysis shown in Figure .

Calcium differs from magnesium in some important respects and these are shown in Figure 3. The calcium detected in the gas stream arises from the carbothermal reduction of the CaO.

$$CaO_{(s)} + C_{(s)} = Ca_{(g)} + CO_{(g)} \qquad (2)$$

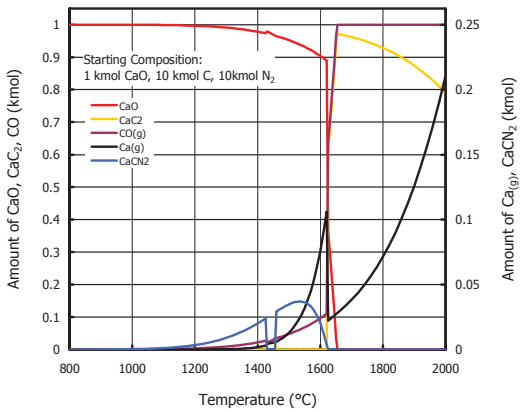

Figure 3: Thermodynamic calculation of the Ca-O-C-N system over a range of temperatures.

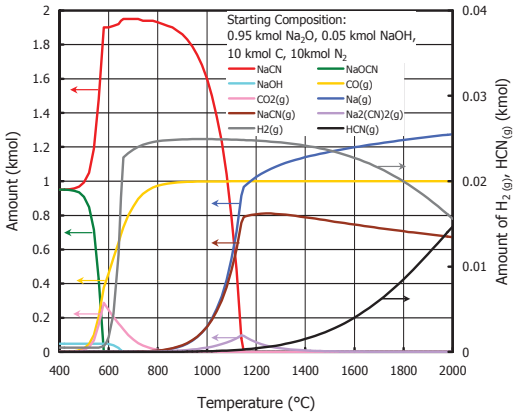

Figure 4: Thermodynamic calculation of the Na-O-C-N-H system over a range of temperatures.

Unlike magnesium, calcium forms a carbide (CaC_2) above about 1600°C by the reaction

$$CaO_{(s)} + C_{(s)} = CaC_{2\,(s)} + 3CO_{(g)} \quad (3)$$

While the carbide is generally stable it can partially decompose with increasing temperature by reaction 4. The carbon would remain with the charge.

$$CaC_{2\,(s)} = Ca_{(g)} + 2C_{(s)} \quad (4)$$

One interesting but unexpected observation from XRD analysis is the presence of calcium cyanamide ($CaCN_2$) in the cooled charge residue. Thermodynamic calculations and the literature [3] would suggest that this results from the reaction of CaC_2 with nitrogen during cooling below 1600°C. While not relevant for continuous operation at high temperature, this reaction would be of concern during plant shutdown for example.

$$CaC_{2\,(s)} + N_{2\,(g)} = CaCN_{2\,(s)} + C_{(s)} \quad (5)$$

Sodium: This was observed at much lower concentrations than either Mg or Ca in the LIBS readings (compare results in Figure with Figure). In contrast to Mg and Ca, sodium is observed at low temperatures (above 800°C). It also shows two peaks; one at 1100-1300°C and another broadly matching the behaviour of magnesium.

The thermodynamic calculations for the reaction of sodium are shown in Figure 4. These differ from the calculations for the other elements in that some NaOH is included with the Na_2O to represent the small amount (about 1-2 wt% after calcination) of water added with the binder during the production of the MgO-C tablets.

The calculations predict that Na_2O is readily converted to NaCN above 600°C by

$$Na_2O_{(s)} + N_{2\,(g)} + 3C = 2NaCN_{(s,\,l)} + CO_{(g)} \quad (6)$$

The NaCN begins to evaporate above 800°C and has completely evaporated by about 1150°C. This could explain the first sodium peak in the LIBS data; an amount of NaCN is produced during the first stage of heating and this subsequently evaporates at 800-1200°C in a burst. Subsequent reaction of the remaining Na_2O proceeds by

$$Na_2O_{(s)} + C = 2Na_{(g)} + CO_{(g)} \quad \text{and} \quad (7)$$

$$Na_2O_{(s)} + N_{2\,(g)} + 3C = 2NaCN_{(g)} + CO_{(g)} \quad (8)$$

Above about 1000°C, $Na_{(g)}$ and $NaCN_{(g)}$ are initially produced in roughly equal proportions but $Na_{(g)}$ begins to dominate as the temperature increases. In a similar manner to magnesium, the reactions become more favoured as the temperature is increased and this would explain the second sodium peak.

One interesting observation is the presence of $HCN_{(g)}$ gas at about 1100°C in small-scale experiments, but not at 1000°C or 1200°C. The thermodynamic calculations predict that $HCN_{(g)}$ begins to be seen at concentrations of 10-20 ppm at about 1100°C. Other experiments have also shown that the temperature for removal of the final water from the charge is also about 1100°C. These reasons explain the narrow temperature window for observation of the HCN gas. However, larger scale carbothermal

magnesium plants would be operated continuously. The thermodynamic calculations show that charging material containing small amounts of moisture into a furnace above about 1200°C could generate gas with significant concentrations of HCN gas.

Silicon: Silicon is the major impurity of similar concentration to CaO. Gaseous reduction products of silica were not produced in sufficient quantity to be detected by the LIBS analyser. One species, $SiO_{(g)}$, can be produced at low concentrations above 1500°C. After reaction at high temperature, the dominant product is silicon carbide by reaction 9 with SiC remaining in the charge and detected by XRD after the experiment.

$$SiO_{2\,(s)} + 3C = SiC_{(s)} + 2CO_{(g)} \quad (9)$$

Aluminium: The reduction products of alumina are the least volatile of the impurities that were investigated and this is reflected in the results in Figure . The modelling predicts conversion of alumina to the nitride (AlN) between 1200°C and 1500°C. Volatile species are $Al_{(g)}$ and $Al_2O_{(g)}$ and these are predicted at low concentrations above 1750°C.

Manganese: The complex behaviour of manganese species in the gas phase that is measured by the LIBS analyser (see Figure) cannot be fully explained by thermodynamic calculations.

Predicted early reduction species include MnO below 1100°C, Mn_4N at 1100-1270°C and manganese metal above 1270°C. Manganese gas could boil off from the metal above about 1300°C before being hidden by the evolution of $Mg_{(g)}$. This would account for the middle peak for Mn but not the other two. Manganese carbonyl could potentially explain the first peak, but calculations would rule that out.

Conclusions:

Real time analysis of the product solids and gases by the LIBS method has proven to be a useful tool in monitoring the progress of reactions in the carbothermal magnesium production experiments. The LIBS technique is being used in the development of a number of other projects at CSIRO.

Thermodynamic modelling has provided useful insights into the behaviour of impurity compounds and can explain a number of the observations generated by the LIBS analysis. The data will prove useful during future scaling up of the carbothermal magnesium process.

References:

1. G. Brooks, S. Trang, P. Witt, M.N.H. Khan, and M. Nagle, “The carbothermic route to magnesium”, JOM, 58, 2006, pp 51-55.
2. G. Brooks, M. Nagle, S. Tassios, and S. Trang, “The physical chemistry of the carbothermic route to magnesium”, Magnesium Technology 2006, Minerals, Metals and Materials Society, Warrendale PA, USA, 2006, pp 25-31.
3. Kirk-Othmer Encyclopedia of Chemical Technology – 4th Edition, John Wiley and Sons, New York, Vol. 7, p 740.

Subsolidus Phase Equilibria of System Cu-Ca-Fe-O

X. Liu, H. Henao, P. Hayes, E. Jak
Pyrometallurgy Research Centre, University of Queensland

Key words: calcium ferrite slags, freeze lining, subsolidus phase equilibria

Calcium ferrite slags described by the Cu-Ca-Fe-O system are used in the continuous copper-converting stage of the Mitsubishi process and the Outokumpu flash converting process. The slags offer a number of advantages over traditional silica-based slags. However they are also highly aggressive and chemically attack conventional refractories; in industry practice the integrity of the furnace wall is maintained through the formation of freeze linings of the slags. Despite the industrial importance of the Ca-Cu-Fe-O slag system, the subsolidus phase equilibria and thermodynamics of the system, which is closely linked to the stability of the furnace freeze lining, have yet to be characterized.

Experimental studies of the Cu-Ca-Fe-O has been made at 1050^{o}C using an isothermal equilibration/quenching/microanalysis approach, and in the region of compositions that are of interest in connection with calcium ferrite slags. The following phases were observed: calcium ferrite phase $4CaO.FeO.4Fe_2O_3$, $CaO.Fe_2O_3$, delafossite $Cu_2O.Fe_2O_3$, spinel primarily Fe_3O_4, two Cu-Ca-Ferrites with composition close to $Cu_2O.2CaO.3Fe_2O_3$ and $Cu_2O.CaO.2Fe_2O_3$, Cu_2O and metallic copper.
The narrow ranges of stability of the Cu-Ca-Ferrite phase particular create difficulties in studying the phase equilibria containing the Cu-Ca-Ferrites. Thus this system was studied by direct measurements of the crystallized phases, and the results analysed and interpreted using thermodynamic principles.

In the present study, the subsolidus phase equilibria of the system Cu-Ca-Fe-O at 1050^{o}C has been constructed for a range of oxygen partial pressure between $10^{-7.0}$ and $10^{-5.1}$ atm. Various tetrahedrons and volumes in compositional space have been identified each of which describes the coexisting phases in equilibrium at selected oxygen partial pressures and temperature. It was concluded that the two Cu-Ca-Ferrites can not be in equilibrium with spinel at metallic copper saturation. The solubility of CaO and Cu_2O in spinel were observed to increase as the oxygen partial pressure increases.

Thermodynamic Modelling of Copper-containing Slags

Taufiq Hidayat, Peter Hayes, Evgueni Jak

Pyrometallurgy Research Centre, The University of Queensland, St Lucia, QLD 4072 Australia

Key words: phase equilibria, copper, silicate slag, thermodynamic database

Copper smelting and converting takes place over a wide range of chemistries and process conditions. Of particular interest in describing these systems are the phase equilibria of silicate-based slags as a function of bulk composition, temperature and gas conditions. The existing chemical thermodynamic databases for these systems[1)] still, however, require improvement to be able to accurately predict the phase assemblages present and their compositions.

The aim of the present study is to optimize the slag solution database ("Cu_2O"-SiO_2-CaO-FeO-Fe_2O_3-Al_2O_3-MgO). This is to be undertaken through: (a) a critical review of existing thermodynamic data; and (b) optimization of FactSage oxide databases with particular focus on Cu-containing systems. The methodology for the optimization involves assessment of thermodynamic properties of pure copper oxide and stoichiometric compounds, and then optimising the parameters in the solution models.

In the presentation, the thermodynamic properties of pure copper oxide and its stoichiometric compounds as a function of temperature are presented. The existing phase diagrams for "Cu_2O" and other oxides (CaO, SiO_2, "Fe_2O_3", Al_2O_3 and MgO) at Cu saturation are presented and discussed, as well as the phase equilibria of slag systems at molten copper saturation with fixed or measured oxygen partial pressures.

The Bragg-Williams, Modified Quasichemical, and GUTS models available in FactSage[2)] will be used to describe the Gibbs free energy excess parameters of the slag solutions, the formalism and advantages of these models are briefly discussed.

The optimized FactSage thermodynamic databases will offer a self-consistent database that provide the ability to predict slag phase equilibria across the full range of process conditions encountered in Cu smelting / converting / slag cleaning.

References

1. S. Decterov and A.D. Pelton, "A Thermodynamic Database for Copper Smelting and Converting", *Metallurgical and Materials Transaction B*, Vol.30B, 1999, pp. 661-670.
2. A.D. Pelton, S.A. Degterov, G. Eriksson, C. Robelin and Y. Dessureault, "The Modified Quasichemical Model I-Binary Solutions", *Metallurgical and Materials Transaction B*, Vol.31B, 2008, pp. 651-659.

Use of Residual Plastic Into Blast Furnaces

Paulo Santos ASSIS[1] , Patricia TAVARES da Silva[2], Maria Lucia FURTADO[3]

[1]Full Professor of Escola de Minas-UFOP, Professor at REDEMAT, Honorary Professor by HUST, Tangshan, China, assis@em.ufop.br

[2]Environmental Engineering Student, ptavares.ufop@gmail.com

[3]Environmental Engineer, mlfurtado@yahoo.com.br

Concerning to the environmental problem of solid residual accumulation in urban waste, this work provides an alternative to plastic recycling, involving industry processes. The object of study consists in plastic materials, which cause serious damage when discharged in environment, specially the Poly (ethylene terephthalate) or PET. The purpose is analysing the feasibility of those products for feeding into blast furnaces tuyeres.

Like proposed by Gorni (2006)[1], fuel value can be attributed to plastic residual in the processes of reducing iron ore in blast furnaces. That proposal seems interesting to the recycling of low or null commercial use residuals, making also possible to replace part of the charcoal in the metallurgic processes for cleaning iron.

PET is a polyester with high resistance to rupture, rigidity, good chemical resistance to abrasion as well as to impact in the oriented form, it has low friction coefficient and minimum oxygen absorption (PARENTE, 2006)[2]. Those features give the material special properties that make it the best and most efficient plastic for the packaging industry, among other uses. This way, there's an intense use of the product all around the world and a consequent expressive generation of residual, which needs to be appropriately treated.

The plastic material injection in blast furnaces is a technique already in use in German and Japanese industries with government support. In those countries the technology demonstrated viability and is seen as an alternative for dealing with waste generation. Some research initially was conducted by (ASSIS, 1999)[3]. It was shown in Perth, Australia, during an International Congress, exposing some results.

Among the three possible ways to recycle PET (energetically, chemically or mechanically) this work focuses on energetic and chemical recycling of the plastic material. The process consists in converting the heat generated when plastic is burned into energy (and uses the gas for contribution in the reduction process) which powers the furnace.

According to Gorni (2006)[1], one of the possible ways to improve the performance of blast furnaces is the injection of coal or oil fines directly into the entry of hot air, since these materials are rich in carbon and complement the supply of this element for the ore reduction process. Pulverized charcoal or mineral coals are the most common substances used in injection through the tuyeres. However, in principle, it's possible to

apply the same method with any material with high hydrocarbons percentage; and PET has high calorific value, which is a positive aspect. Comparisons with chemical analyses of coal, oil and plastic show similarities in these products, according to different characteristics.

The aim of the work is to evaluate the viability of recycling PET (as product after consumption) and use of its energy to reduce iron in blast furnaces. To achieve this goal, a sampling was held, collecting recycled and pulverized PET, carrying its characterization (using the Scanning Electron Microscope or MEV, as a tool) considering the grain size distribution; besides porosity, adsorption and density analysis (using the methods Nitrogen Absorption – BET and Helium Gas Multipycnometer), analysis of combustibility rates through simulation blast furnace with injection of samples containing different percentages of coal and PET. The gases generated in the process were determined in the ORSAT analyzer.

The results of punctual chemical analysis of particles using MEV detected concentrations of aluminium, bromine and silicon, indicating contamination. That is very likely, since the sample analysed is after-consumption material; but at the same time, proves the inviability of use of some recycling processes in cases of food package fabrication, for example. Moreover, a difference of porosity between the coal and PET was identified, once the coal is more porous than the plastic material analyzed. Porosity indicates the reactivity level of the product during the firing process, because of the contact area between the material surface and the gases. Consequently, most results found in the samples containing PET showed values of burning rates slightly lower than samples containing coal. However, it's important to note that, for the injection rate of 100 kg/ton hot metal generated, the samples containing 40% and 20% PET showed a combustibility rate higher than the one correspondent to 100% coal, as can be seen in tables 1 and 2 below.

Table 1: Preliminary results from furnace simulator

COMBUSTIBILITY RATE			
Rates of material injection			
	50 kg/ton	100kg/ton	150kg/ton
Plastic	**Amount in the trial**		
(%)	**0.050 g**	**0.100 g**	**0.150 g**
100	87.4	84.85	74.55
80	89	86.8	76.7
60	90.9	88.7	78.15
40	93.2	91.55	78.65
20	93.9	92.1	78.2

Table 2: Results of combustion rate for samples of coal

COMBUSTIBILITY RATE			
Rates of material injection			
	60 kg/ton	100 kg/ton	120 kg/ton
coal	**Amount in the trial**		
(%)	**0.060 g**	**0.100 g**	**0.120 g**
100	95.2	88.2	81.9

It’s also important to observe that the percentage increase of plastic in the mixture injected into the simulator caused a reduction in the rate of burning. That’s probably due to consequent decrease of the relation between oxygen and carbon concentrations in the burning zone, and also because of coal burning power, which is larger than the plastic.

Although the results obtained for the mixture with plastic material demonstrate parameters no more advantageous than the one correspondent to the coal alone, the application of the technique presented is still considered feasible, since, depending on the percentage of each material, the differences between values are small and not significant. Besides, the combustion rates are still considered satisfactory for the function. Recalling the most important aspect of the work is the viability of replacing part of the coal by residual plastic.

References:

[1] GORNI, A.A. Aproveitamento de Plástico Pós-consumo na Forma de Combustível para Altos-fornos e Coquerias. Revista Plástico Industrial, pág 84-100, 2006.

[2] PARENTE, Ricardo Alves. Elementos Estruturais do Plástico Reciclado. Dissertação (Mestrado). USP – Universidade de São Paulo, 2006.

[3] ASSIS, P.S. et alli. Some Thoughts about Injection of Plastics into the Blast Furnace. Presented in the International Congress on Alternative Routes of Iron and Steelmaking-ICARISM. Perth, Australia, Sept 1999, 5p.

Acknowledgments:

This work wouldn't be possible without the support of CNPq, which assisted all the research process and also helped on the trip to Australia. I would also like to express my gratitude to the universities Universidade Federal de Sao Carlos and Universidade Federal de Ouro Preto, where the research was conducted. And it's also important to mention the always helpful leadership of Prof. Assis, without whom all this wouldn't happen.

Efficient Utilisation of Coal by Integrating Various Industries

Guangqing Zhang

School of Materials Science and Engineering, the University of New South Wales

Key Words: Coal utilisation, energy efficiency, integration of energy systems

Natural gas, petroleum and coal are hydrocarbons with significantly different molecular weights and hydrogen to carbon ratios. Among the three conventional fossil fuels, coal is the most abundant and the cheapest, while petroleum is a most desirable fuel resource because it is easily processed into valuable petroleum products, especially gasoline and diesel. How to utilise coal resources, especially as a replacement of petroleum, is an important topic.

Significant resources have been devoted in research and development of technologies for production of petroleum substitute from coal. There are three technical routes to convert coal into petroleum substitute: Fischer-Tropsch (FT) process, direct coal liquefaction by hydrogenation, and pyrolysis. Among them, pyrolysis is a simple process with mild reaction conditions and low capital investment, but is with the disadvantage of a relatively low yield of total gas and liquid, below 50%. The main problem for a large scale commercialisation of this technology is an efficient utilisation of the liquefaction residue, i.e. char.

Integration of various industries can provide an ideal solution for efficient utilisation of coal. This includes processing coal by pyrolysis with production of liquid and solid fuel products, which can be further processed into final products in petroleum refining/petrochemical industry. The solid char generated in coal pyrolysis can be used in metallurgical industry, especially for injection in blast furnace ironmaking process. Char can also be used as fuel for power industry by replacing coal.

A schematic flowsheet of complex utilisation of coal in various industries is presented in Figure 1.

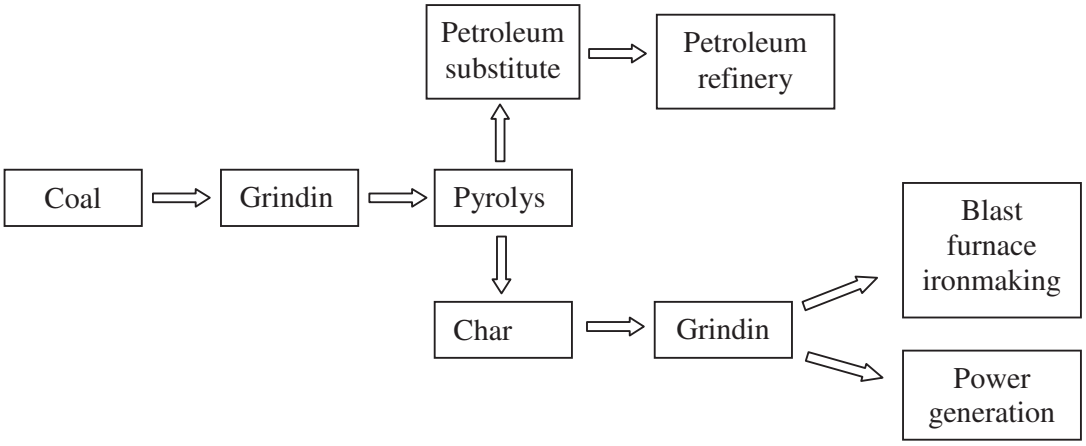

Figure 1. Schematic flowsheet of combined utilisation of coal for petroleum substitute production, ironmaking and power generation.

Pyrolysis process can be carried out at ambient pressure and temperature of 550-650 °C. A review of different technologies for coal pyrolysis can be found in a monograph[1]. Figure 2 illustrates a fast pyrolysis process proposed in literature[2] and the change of recovery of liquid fuel with pyrolysis temperature and time. In this process, heat of pyrolysis is provided by partial combustion of char. This process is very simple and cost-efficient.

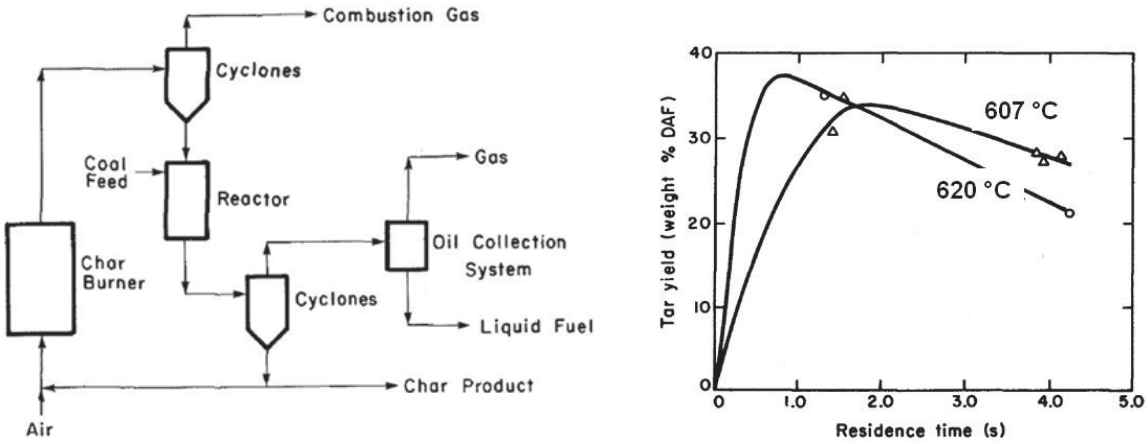

(a) (b)

Figure 2. Schematic flowsheet of a coal pyrolysis process (a) and the liquid fuel yield (b)

Current blast furnaces and coal fired power generation plants use pulverised coal as fuel. Using pulverised char to replace pulverised coal will provide the following advantages to these processes: (1) saving energy of coal grinding and enhancing combustion efficiency; (2) increasing the safety of the pulverisation operation and pulverised char storage, and making the transport of the carbonaceous materials more reliable; (3) potentially, replacing pulverised coal injection by injecting char may make blast furnace operation more stable and more productive; (4) increasing the completeness of combustion of carbon.

Integration of various industries in coal utilisation provides a route for efficient utilisation of coal resources which does not need high investment in technology development and building up new plants, and will generate significant economic benefits to the industrial operators. This is especially important when the related industries are under the pressure of increasing their operation costs under the Carbon Trade Systems.

References

1. Gavalas G.R. *Coal Pyrolysis*. Elsevier Scientific Publishing Company, Amsterdam, 1982.
2. Jin H.G., Xua Y. and Lin R. (2008) *International Journal of Hydrogen Energy*, 33, 9-19.

Exergy Balance of Pulverized Coal Injection Into Blast Furnaces

Paulo Santos ASSIS [1], Giane Aparecida da SILVA [2], Tiago Luis de OLIVEIRA [3], Antônio Carlos MENEGHIN [4]

[1] UFOP, Full Prof.of Escola de Minas-UFOP, Prof at REDEMAT, Honorary Prof by HUST, China, assis@em.ufop.br
[2] Production Engineer, Grad. Student at REDEMAT, gianeapasilva@yahoo.com.br
[3] Mechanical Eng. Grad. Student at REDEMAT, tiagoluiscg@yahoo.com.br
[4] Geology Engineer, Ligas de Alumínio S/A-LIASA, geo@liasa.com.br

In thermodynamic, the exergy of a system is defined as the maximum useful work that can be obtained from the process at a given state in a specified environment.[1] The injection of pulverized coal is a worldwide technique, because it reduces the cost of the production in the blast furnace through the reduction of coke rate or even charcoal rate.[2] In this paper it is sought to quantify the exergy potential through the irreversibility factors related to the operation fluctuation into the blast furnaces tuyeres, so to estimate potential financial earnings, arisen from the reduction of exergy losses.

The model presented is based on computational algorithm for calculating the exergy loss in the "raceway" of a blast furnace. Using Microsoft Excel as a tool for the application of thermodynamic calculations, we could simulate the operational parameters of a blast furnace and submit these to the calculation of exergy and analyze the types of losses in the process under different conditions of coal injection.

First, a model system was obtained: in our context the blast furnace is considered as an open system, being selected the "raceway" as a control volume, aiming at the understanding of irreversible phenomena inherent to this region. In order to quantify the exergy losses in the combustion zone of a blast furnace, the temperature of the gas that leaves the raceway, the irreversible work, the entropy generated and the exergy destroyed should be determined. However, before running the calculations certain criteria must be considered. It is measurable that the flow conditions occur in steady state, the air and gases involved in combustion are considered ideal. It is interesting that the changes in the kinetic and potential energies are negligible and the combustion is incomplete, and a conducted mass balance that allows the calculation of the number of mols of the elements involved in the reaction according to the operational parameters of the process. Finally the combustion zone is considered adiabatic, thus it does not exchange heat with its surroundings.

After quantifying the number of moles of the reactants and the products in the combustion zone, we could identify the total entropy of input and output. For this we used thermodynamic tables, taking as parameters the inlet temperature as the

temperature and wind output temperature as the flame temperature. The latter being calculated by the following formula:

$$T_{Flame} = 1267{,}9 + 0{,}9742T + 57{,}636E - 7{,}146U - 2T_{ICP} \quad \textbf{(1)}\ [3]$$

Irreversibility or lost work generated by chemical reactions, friction, heat transfer with finite temperature difference always generate entropy and consequently the destruction of exergy, thus:

$$X_{destroyed} = T_0 \overline{S}_{ger} \geq 0 \quad \textbf{(2)}$$

The maximum work that can be performed in a combustion process, called exergy or availability may be limited by the reversible work. Given the conditions in which it is considered that reactants and products are in equilibrium temperature of the Gibbs function becomes significant.

$$W_{rev} = \sum N_R \overline{g}_R - \sum N_P \overline{g}_P \quad \textbf{(3) [1]}$$

Through operational parameters obtained from a hypothetical blast furnace (table 1), it was measured in loss rate for three operating conditions, as can be seen in Figure 1. It is observed that the situation 2 is equivalent to the real operation of the selected blast furnace, where there is no variation of injection rate. In the situation 1 and 3, then a variation of injection rate for one blast furnace was done considering certain planned parameters for operation. It appears that with the increase of coal injection, there is an increase of availability and a reducing of exergy damages, consequently the increase of rate of injection characterizes a reduction of the rate of damage. According to Assis [3], the economy obtained by injection into the blast furnace is showed by:

$$E_T = TIMP.(CMS.TS - CMI).P \quad \textbf{(4)}$$

Then, attributes the value of 180 USD/t for CMS, 1 38 USD/t for CMI and TS of 0, 9, the formula can be used for additional economy, for a possible exergy loss next to zero. The results indicate that when one considers the exergy losses in the tuyeres, an increasing in the economy of the process from 425 to 597 USD can be expected, when it is considered a PCR by 140 kg/t. That means an additional economy of 5232961 annual USDollars, for each 140 kg/t hot metal. When 200 kg/t hot metal is injected, then an additional economy can reach values by the order of 7357920 annual US.

The model showed satisfactory results of calculus and its use may be of fundamental importance in the everyday operation of a blast furnace, since it predicts heat loss that can put forth the process stability. It is interesting to consider that, by the exergy analysis one can improve results obtained by the powder injection rate.

Figure 1

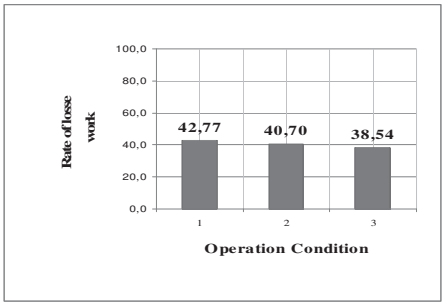

Fig. 1 Rate of losses work

Table 1: Conditions of an operating blast furnace

	Fuel		Characteristic of blowing				Characteristic of coal		
Situation	Coke rate kg/t	PCR kg/t	Flow Nm³/min	Temp. °C	Umid. g/Nm³	Enrichment of O_2 %	C %	%H_2O	MV %
1	343,03	**80**	2288	1090	17,1	1,51	72,7	0,98	16
2	343,03	**140**	2288	1090	17,1	1,51	72,7	0,98	16
3	343,03	**200**	2288	1090	17,1	1,51	72,7	0,98	16

Acknowledgments

The authors would like to acknowledge FAPEMIG and CNPq for helping the professor in the research conducted so to CNPq a part of financing the trip to Australia.

References

1. ASSIS, C.F.C.; Caracterização de carvão vegetal para a sua injeção em altos-fornos a carvão vegetal de pequeno porte. Ouro Preto: REDEMAT, 2008.
2. ASSIS, P.S. Injeção de Materiais Pulverizados em Altos-Fornos. São Paulo: ABM, 2003.
3. ÇENGEL, Y.A.; BOLES, M.A. Termodinâmica. São Paulo: McGraw-Hill, 2006.

Effect of Impurities on Gasification of Graphite

Jing Zhang, Guangqing Zhang and Oleg Ostrovski

School of Materials Science and Engineering, the University of New South Wales

Key words: Gasification, graphite, impurities, iron, catalysis

Gasification of carbonaceous materials is an important category of reactions in metallurgical processes. Carbon in different forms (graphite, coke, coals) reacts with hydrogen, water and carbon dioxide at high temperatures to produce gaseous methane, hydrogen, and carbon monoxide. In ironmaking blast furnace, gasification reaction does not only provide the reducing gas, but also affects the coke degradation. It may reduce coke strength and deteriorate the permeability of the solid burden with a negative effect on the blast furnace productivity. Carbon gasification reaction also plays an important role in the carbothermal reduction of metal oxides. Therefore, further understanding of the gasification reactions under specific conditions of metallurgical processes is paramount to development of these processes.

The gasification reaction is influenced by the reaction conditions and the properties of the carbonaceous materials. In this study, pure graphite was used as a standard material to establish effects of various factors on the gasification reaction.

Gasification of graphite was studied in a fixed bed reactor in the CO_2-Ar gas mixture. Graphite powder was pressed into a thin disk of 8 mm diameter and about 2 mm thick, weighing approximately 0.15 g, which was loaded into a reaction tube and reacted with CO_2-Ar gas mixture which was introduced into the reactor at the flow rate of 1 NL/min The reaction experiments were carried out isothermally. The composition of the off-gas was monitored online by an infrared gas analyser. The apparent gasification rate was calculated from the CO content of the off gas.

The effect of temperature on the gasification rate was examined in the range 900°C to 1500°C. The apparent reaction rate curves at different temperatures are presented in Figure 1. The rate of reaction increased in the early stage, and then started to decrease with further reaction. The initial increase in apparent reaction rate was attributed to the increase of surface area of graphite by enlargement of the existing micropores and generation of new micropores. As gasification proceeded, the micropores were further enlarged and coalesced causing a reduction of surface area, and resulting in reduction in apparent gasification rate.

Overall, the rate of gasification tended to increase with increasing reaction temperature. However, there was an abnormity between 1200 °C and 1100 °C, which was attributed to the effect of impurities in the graphite, which was examined further.

3 wt% of different metal oxides were added to graphite individually to examine their effects on the rate of gasification. TiO_2 and Al_2O_3 had no catalytic effect on the graphite gasification; moreover addition of these oxides slightly decreased the gasification rate. Addition of SiO_2 also had a weak effect. Fe_2O_3 and MnO enhanced the apparent gasification rate significantly, particularly at the early stage.

Figure 2 presents the gasification curves of graphite with and without addition of 3 wt% of metallic iron powder at 1100 and 1200 °C, respectively. Apparent gasification rate was significantly increased by addition of the metallic iron. Graphite contained close to 2000 ppm iron. Iron in graphite catalysed the gasification reaction, which was stronger at 1100°C than at 1200°C due to melting or sintering of iron particles which may decrease their surface area and active sites. The morphology of iron particles before and after reaction was observed by SEM. Iron particles were dispersed uniformly in the graphite pellet, with particle size 1-4 μm. After gasification experiments at 1200 °C, iron particles formed clusters, or nodules. In contrast, the iron particles after gasification at 1100°C were of almost the same size as before the gasification test.

An effect of CO_2 on the gasification rate was studied at 1100 °C and 1400 °C. The apparent rate of gasification increased with increasing CO_2 partial pressure at both temperatures.

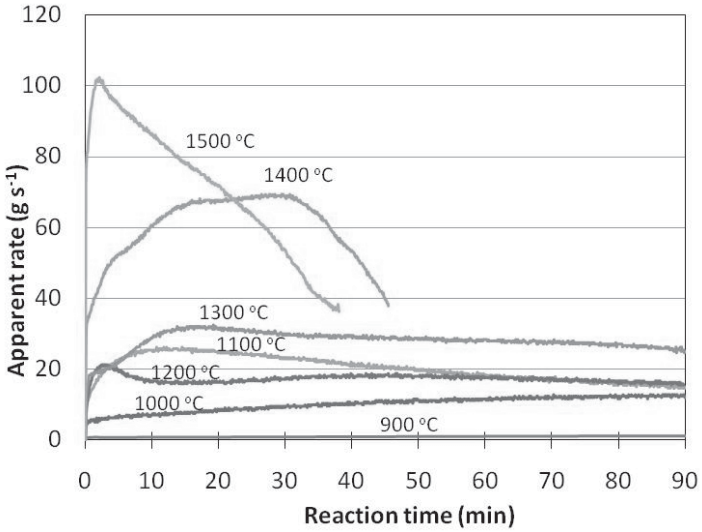

Figure 1. Effect of temperature on the gasification rate. CO_2 partial pressure: 6 kPa.

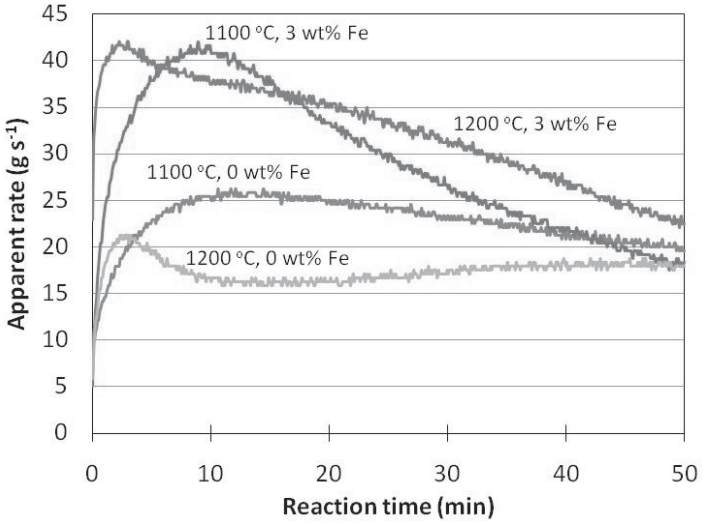

Figure 2. Effect of metallic iron addition (3 wt%) on the gasification rate. CO_2 partial pressure: 6 kPa.

Flow of Liquid Slag through Coke Channels

Hazem F. Labib[1], Brian J. Monaghan[1], Raymond J. Longbottom[1], Sheng J. Chew[2] and Peter R. Austin[2]

[1]PYROmetallurgical Group, Faculty of Engineering, University of Wollongong, Wollongong, NSW 2522, Australia.
[2]BlueScope Steel Research, P.O. Box 202, Port Kembla, NSW 2505, Australia.

Keywords: Coke, Slag, Blast Furnace, Capillary

The blast furnace is the primary liquid iron production unit for the majority of the world's steel. At present, our knowledge of the blast furnace does not extend to a full description of the material flow, chemistry and internal physical structure of the furnace. This is due to the highly complex inter-dependent thermal, physical and chemical phenomena within the furnace, and to limited access to the furnace to observe important phenomena directly. This study is focused on developing an improved understanding of liquid flows in the lower zone of the blast furnace. To this end, two experimental methods have been developed in which the molten slag flow through a laboratory scale coke bed and the flow through a narrow channel in coke are studied. The lower zone of a blast furnace may be approximated to a packed bed. Therefore, fundamental studies of liquid flows in a packed bed and channels developed between packed coke particles should offer insights into blast furnace performance and operation.

To minimise the effect of the inherent heterogeneity in coke obfuscating experimental results a synthetic coke (coke analogue) has been developed[1,2] and used in the aforementioned experimental methods. In the coke analogue, the porosity, mineralogy and mineral phase dispersion throughout the coke has been controlled and characterized[3].

In this extended abstract, preliminary results of the flow of molten slag through coke channels are presented and discussed.

Experimental

In order to simulate the flow of slag between the inter-particle voids of a coke bed the experimental set up given in Figures 1 and 2 was used. A funnel shaped cavity (Figure 1) with a channel was cut in a coke analogue sample. A pressed and sintered slag pellet was placed in the funnel cavity. The analogue and slag were heated under argon in an electrically heated furnace (Figure 2) and the slag melted. After cooling, whether the slag flowed through the channel and any interaction the slag had with the analogue were characterized. This procedure was carried out for a number of slag and coke analogue compositions and different channel diameters. The experimental conditions used were 1500°C, with a dwell time at temperature of 30 minutes, a purified Argon flow rate of 1 L/min and slag and coke analogue compositions as given in Tables 1 and 2. The slag compositions chosen were based on what might be expected in the lower zone of a blast furnace and to exclude the effects of oxidation of the coke analogue with FeO.

Slag pellets were prepared from laboratory grade oxides and sintered at 800°C. Coke analogue funnels were machined and their channel diameters confirmed using optical microscopy.

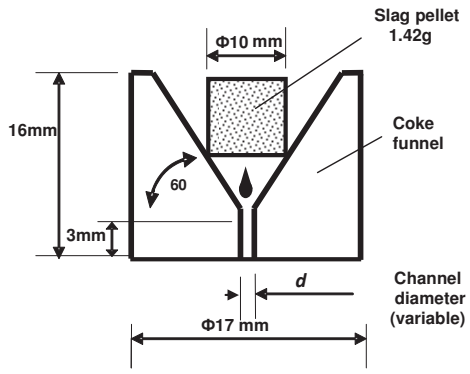

Figure 1 Schematic presentation of the flow of slag through a coke channel

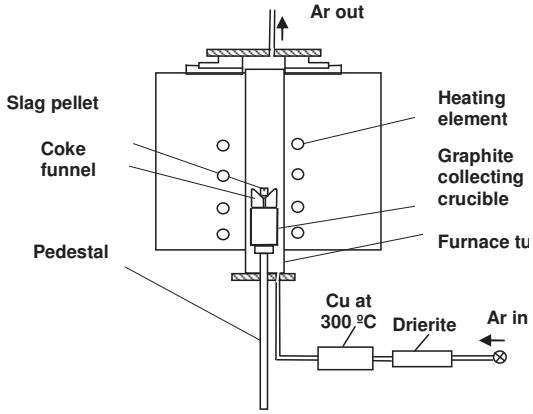

Figure 2 Schematic diagram for the apparatus for the dripping experiment

Table 1. Slag compositions and viscosity used in this study.

Slag	Initial slag composition in Mass pct					Viscosity at 1500ºC, Pas (calculated[4])
	CaO	SiO_2	Al_2O_3	MgO	V ratio	
A	40.7	37.4	12.5	8.8	1.1	0.26
B	44.0	34.5	12.2	8.8	1.3	0.18

Table 2. Coke Analogue compositions used in this study.

Designation	Mineral type	Minerals Content in Mass pct
COKAN	No minerals	0.0%
COKAN-CA1	$CaO.Al_2O_3$	4.4%

Results

Preliminary results showed that slag A flowed through channels of diameters ≥4.4 and ≥5.0 mm for COKAN-CA1 and COKAN respectively. Slag B flowed through channels ≥5.0 and ≥4.4 mm for COKAN-CA1 and COKAN respectively and only partially flowed through a channel of 4.4mm for COKAN-CA1. Channel diameters lesser than these values showed no slag flow through the channel.

Examination of the interface between slag and coke analogue revealed that slag had penetrated the surface open pores of the coke analogue. A Typical micrograph and SEM-EDS analysis for two major elements in slag (Ca and Si) at the interface is shown in Figure 3.

Fukutake *et al*[5] described six major forces that act on the liquid that flows through packed bed in general. By eliminating forces related to motion and gas effect, we obtain the forces acting on a liquid phase statically suspended at the top of an inter-particles' void as described by Husslage [6] and given in equation 1.

$$\rho g h = -\frac{4\sigma \cos\theta}{d} \qquad (1)$$

where, □ is slag density, g is gravitational acceleration, σ is the surface tension of the slag, θ is the contact angle between slag and coke analogue, d is the channel diameter and h is the molten slag head over the opening tip (12 mm in experimental setup used).

This equation is based on the force balance between the weight of the liquid slag and the capillary repulsion force. At a certain channel diameter, the liquid slag hydrostatic pressure overcomes the capillary pressure and the slag starts to flow through the channel. This is analogous to case of applying the Young (1805) equation to the process of infiltration of liquids into porous media where the porosity assumed cylindrical and open[7]. Using characteristic values for □[4], σ[4] and θ[6] in equation 1, *d* can range from 2.6 to 5.4 mm. The critical *d* values measured in this study lie within this range.

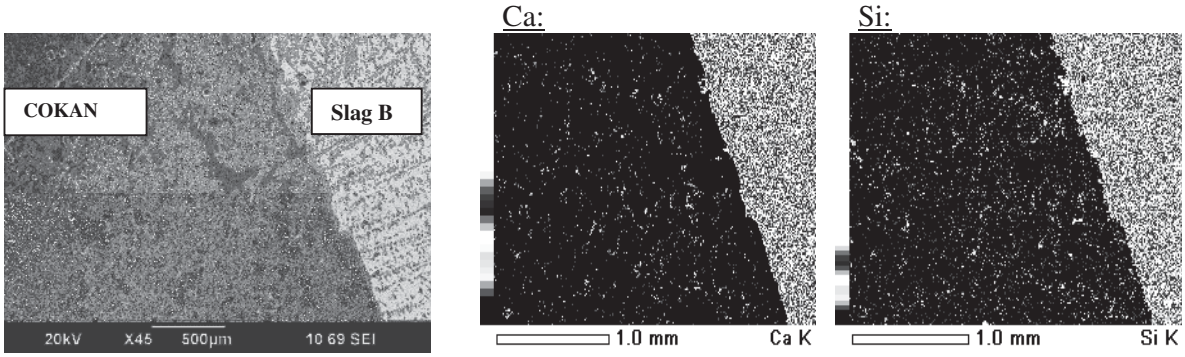

Figure 3 Micrograph of SEM and SEM-EDS analysis for Calcium and Silicon at the interface between slag B and COKAN

Conclusions

The flow of slag through channels of synthetic coke (coke analogue) at 1500ºC revealed that there is a minimum channel diameter needed to allow slag to freely drip. In this work, the minimum channel diameters were between 4.4 and 5.0 mm for the combinations of slags and cokes examined. The results were in good agreement with a simple force balance analysis based on gravity and capillary forces. Further extension of the experiment is needed to cover other combinations of slag and coke compositions.

Reference

1. Monaghan, B.J., Chapman M.W., Nightingale, S.A.: Carbon Transfer in the Lower Zone of a Blast Furnace, Seetharaman Conference, Materials processing towards properties, June 2010, Sigtuna, Sweden.
2. Monaghan, B.J., Chapman M.W., Nightingale, S.A.: Carbon Transfer in the Lower Zone of a Blast Furnace,, Steel Research International, V81, pp829-833
3. Chapman, M. "Insoluble oxide product formation and its effect on coke dissolution in liquid iron." PhD Thesis, University of Wollongong,2008
4. KC Mills, Slags Model version 1.07, National Physical Laboratory, UK, 1991
5. Fukutake, T. and V. Rajakumar, "Liquid Holdup and Abnormal Flow Phenomena in Packed Beds Under Conditions Simulating the Flow in the Dropping Zone of a Blast Furnace," Trans. Iron Steel Inst. Jpn, Vol. 22(5),1982,May,pp. 355-364.
6. Husslage, W. M. "Dynamic distributions: Sulphur transfer and flow in a high temperature packed coke bed ". Doctoral Thesis, Delft University, NL,2004
7. Eustathopoulos, N., M. G. Nicholas and B. Drevet "Wettability at high temperatures", Oxford :, Pergamon, 1999.

Investigation of Freeze Linings formed during Copper Smelting

Ata Fallah Mehrjardi, Peter Hayes, Evgueni Jak
Pyrometallurgy Research Centre, University of Queensland

Keywords: Freeze Linings, Copper Smelting

Freeze-linings are being increasingly used in industrial pyrometallurgical processes to ensure the maintenance of furnace integrity in increasingly aggressive environments. Steady state heat transfer models have been developed to predict the thicknesses of the deposits. The existing models do not, however, take into account potential effects of the chemistry of the systems. In the current research the formation of freeze linings is being studied under controlled laboratory conditions. Synthetic slag contained in a refractory crucible is heated in an induction furnace. An air-cooled ”cold finger” is submerged in the rotating bath. The effects of bath composition, forced convection and superheat on the morphology and thickness of freeze-lining is being investigated. To understand the processes occurring during the development of the deposit, some experiments are also carried out for different submergence times. The solidification, heat and mass transfer processes that are occurring during freeze lining formation are discussed.

Influence of Density Differences and Bottom Bubbling Conditions on Formation of Metal Emulsions

Duk-Yong Song[1], Nobuhiro Maruoka[2], Hiroyuki Shibata[2], Shin-ya Kitamura[2]
Naoto Sasaki[3], Yuji Ogawa[3] and Michitaka Matsuo[3]

[1]Graduate School of Engineering, Tohoku University, 6-6 Aoba, Aramaki, Aoba-ku, Sendai 980-8579, Japan
[2]Institute of Multidisciplinary Research for Advanced Materials, Tohoku University, 2-1-1 Katahira, Aoba-ku, Sendai 980-8577, Japan
[3]Nippon Steel Corporation, 20-1 Shintomi, Futtsu, Chiba 293-8511, Japan

Keywords: steelmaking, refining, metal emulsion, interfacial area, bottom bubbling

1. Introduction

In the steelmaking process, metal/slag droplets are dispersed in a slag/metal phase by gas injection or mechanical stirring. Metal emulsions, in which metal droplets are dispersed in the slag phase, is a useful way to improve the reaction rate by increasing the reaction interfacial area between the metal and the slag phases.[1-2] In a previous study, the influence of the gas flow rate on metal emulsion formation was investigated using a Pb-salt system.[2] It was determined that the amount of metal emulsion increases with the flow rate of the bubbling gas up to a maximum value. However, the density difference between the Pb and salt phases in this system is higher than that between the phases of the iron-slag system. Therefore, in this study, an Al-5%Cu alloy and chloride salt were used as the metal and slag phases to investigate the influence of the density difference on metal emulsion formation.

2. Experimental Methods

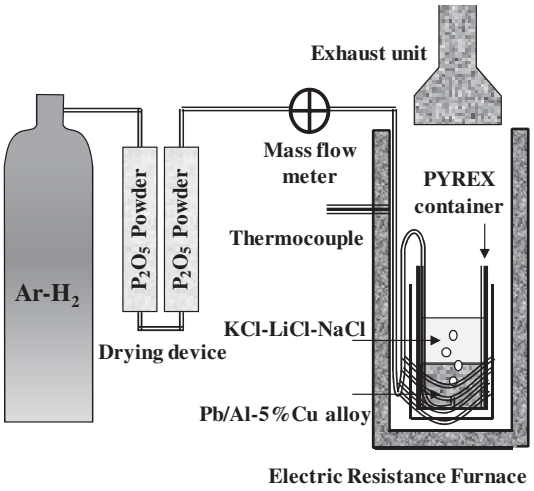

Fig.1 Schematic diagram of experimental apparatus

Figure 1 shows the experimental apparatus used in this study. Table 1 shows the experimental conditions and properties of materials as compared to those in the previous study.[2] 450 g of Al alloy and 300 g of chloride salt were melted in a Pyrex

container (60 mm φ × 180 mm) at 923 K, following which Ar-3%H_2 mixed gas was injected from the center of the bottom of the container. After bubbling initiated, approximately 1 g of salt was sampled at the center of the molten salt phase at certain intervals until 30 min had elapsed. The salt samples were then dissolved in water, from which the metal droplets were separated using a membrane filter with a pore size of 2 μm. The total surface area was calculated from the number and sizes of the metal droplets, which was determined using a digital microscope.

Table 1 Experimental conditions and properties of materials.

	Metal phase		**Slag phase**
	Al alloy	Lead [2]	Fused salt
Compositions	Added 5%Cu	99.999 %	KCl-LiCl-NaCl = 50:42.1:7.9 mass %
Melting Point (K)	919	603	628
Working Temp. (K)	973	723	Depends on metal phases
Density (g/cm^3)	2.7	11.3	1.9
Properties	Low density	High density	Water soluble, does not react with metal and transparent

3. Results

A large number of Al droplets were measured with sizes ranging from 2–100 μm in diameter. Figure 2 shows the influence of bubbling time on the total surface area of

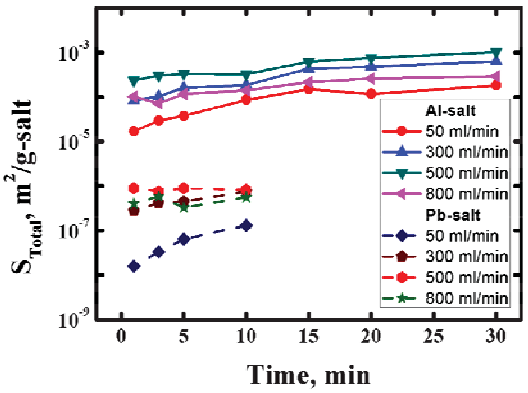

Fig. 2 Influence of gas flow rate on total surface area of metal droplets as a function of bubbling

metal droplets as compared to the Pb-salt system. At each gas flow rate, the total surface area increased with time and reached a steady state approximately 30 min after bubbling initiated. The surface area of the Al alloy system is several times higher than that of the Pb-salt system. This is because the density of the Al alloy is 5 times lower than that of Pb, leading to a long residence time of the Al droplets in the molten salt phase. Figure 3 shows the influence of the gas flow rate on the total surface area in the Al alloy-salt system as compared to the Pb-salt system. Samples were taken 10 and 30 min after

bubbling initiated. The total surface area of Al droplets increased with the gas flow rate

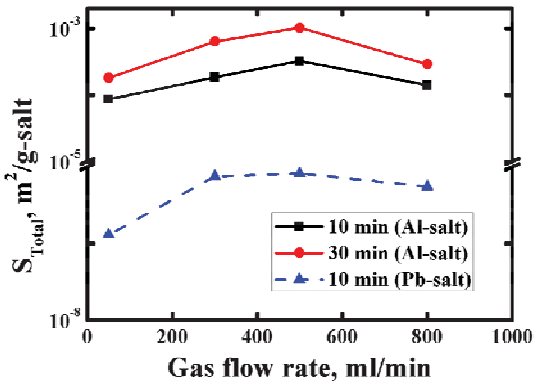

Fig. 3 Influence of gas flow rate on the total surface area of metal droplets as compared to a Pb-salt system

and reached a maximum value at a gas flow rate of 500 ml/min, beyond which it decreased. This trend mirrors that of the Pb-salt system, although the density difference between the Al alloy and the salt is not the same as that in the Pb and salt system.

4. Conclusion

The influences of density difference and bottom bubbling rate on the formation of metal emulsion were determined by comparing an Al alloy-salt system and Pb-salt system. The surface area of the metal emulsion in the Al-salt system was much larger than that in the Pb-salt system because of the density differences of the metal phase. In contrast, the trends of emulsion formation as a function of gas flow rate in both systems are the same despite the differences in the densities of the metals.

References

1. F. Oeters, *Metallurgy of steelmaking*. VSHD, Berlin, 1994, pp.284.
2. D.Y. Song, N. Maruoka, T. Maeyama, H. Shibata, and S. Kitamura, "Influence of Bottom Bubbling Condition on Metal Emulsion Formation in Lead-Salt System," *ISIJ International*, Vol.50, No.11, 2010, pp. 1539-1545.

Viscosity Modelling for Fully Liquid Slags containing Fe_2O_3 using a Quasi-Chemical Viscosity model

Mao Chen, Masanori Suzuki, Evgueni Jak
Pyrometallurgy Research Centre, University of Queensland

Keywords: viscosity model, Eyring equation, structural units, Fe_2O_3

Slag viscosity is a property essential for the metallurgical processes. Development of a reliable and general model, which enables the viscosity of multi-component slag systems to be predicted over a wide range of slag compositions and temperatures, is demanded for the improvement of efficiency and reduction of the cost and energy consumption in the copper production.

From critical literature reviews of the viscosity data of fully liquid slags used in copper production, it is clear that one of main components -- Fe_2O_3 has not been well investigated experimentally and there is no accurate viscosity model describing the effect of Fe_2O_3. The results vary and cannot show a clear tendency. In the present study, a structurally-based quasi-chemical viscosity model is being developed in the fully liquid slag containing SiO_2, CaO, Al_2O_3, FeO and Fe_2O_3 over the whole range of compositions and temperatures. The Eyring equation [1] is used to express viscosity as a function of temperature and composition.

$$\text{Eyring equation:} \quad \eta = \frac{2R\sqrt{2\pi k}}{\Delta E_v} \frac{m_{SU}^{1/2}}{v_{SU}^{2/3}} T^{\frac{3}{2}} \exp\left(\frac{E_a}{RT}\right)$$

The model uses the change of activation and vaporization energies of different structural units to show the change of the viscosities. The model links the slag internal structure through the concentrations of various $Si_{0.5}O$, $Me^{n+}{}_{2/n}O$ and $Me^{n+}{}_{1/n}Si_{0.25}O$ viscous flow structural units. The concentrations of these structural units are derived from a quasi-chemical thermodynamic model of the liquid slag using FactSage computer package and ChemApp software. From 1st rule in Pauling's principle and some other similarities, the model was constructed by assuming the similar behaviour of Fe_2O_3 as Al_2O_3 having the charge compensation effect in oxide melts. The predicted viscosities are within the experimental uncertainties. The validity and limitations of the present model were also discussed.

Viscosity experiments in a wide range of Fe_2O_3 concentrations were proposed to verify the assumptions in the modelling study. This research will improve the understanding of the behaviours of the slag viscosity and get a new methodology for development of slag viscosity models in complex system which can be progressively extended to all slag systems described by a quasi-chemical thermodynamic model.

References

1. H. Eyring, "Viscosity, plasticity, and diffusion as examples of absolute reaction rates", J.Chem. Phys., Vol.4, No. 238, 1936, pp. 283-291

Reaction Mechanism of Carbothermal Synthesis of Silicon Nitride

Xiaohan Wan, Guangqing Zhang, Hal Aral, Oleg Ostrovski
School of Materials Science and Engineering, the University of New South Wales

Key words: Carbothermal synthesis, silicon nitride, silicon carbide

Silicon nitride (Si_3N_4) finds wide industrial applications due to its high strength over a board temperature range, moderate thermal conductivity, low coefficient of thermal expansion, high elastic modulus, and high fracture toughness. This work investigates carbothermal synthesis of Si_3N_4 by reduction of silica.

Carbothermal synthesis of silicon nitride was examined by heating the pellets of a silica-graphite mixture with a molar carbon/silica ratio of 4.5, in an atmosphere of nitrogen or nitrogen-hydrogen gas mixture. Carbon monoxide evolution rate from the reduction reactions was monitored by a gas analyser. The oxygen, nitrogen and carbon contents in the reduced samples were measured by LECO analysers, from which the extents of reduction and nitridation of the reduced samples were calculated.

Carbothermal reduction of silica in nitrogen atmosphere takes place through a number of complex reactions and leads to SiC (silicon carbide) and Si_3N_4 formation:

$$3SiO_{2(s)} + 6C_{(s)} + 2N_{2(g)} = Si_3N_{4(s)} + 6CO_{(g)} \quad (1)$$

$$SiO_{2(s)} + 3C_{(s)} = SiC_{(s)} + 2CO_{(g)} \quad (2)$$

SiC reacts further with nitrogen and silica to form Si_3N_4 as shown in reactions (3) and (4):

$$3SiC_{(s)} + 2N_{2(g)} = Si_3N_{4(s)} + 3C_{(s)} \quad (3)$$

$$2SiC_{(s)} + SiO_{2(s)} + 2N_{2(g)} = Si_3N_{4(s)} + 2CO_{(g)} \quad (4)$$

Figure 1 shows the distribution of silicon in different compounds in the progress of reduction at 1723K. It was assumed in the calculations that all nitrogen and oxygen measured by LECO existed in the form of Si_3N_4 and residual SiO_2, and rest Si in reduced samples was in the form of SiC. Part of the silicon was lost from the sample as gaseous SiO, which was determined from the mass balance.

In the early reduction stage, silica was predominantly converted to SiC, which was further converted to silicon nitride. Conversion of SiC to Si_3N_4 was confirmed using SiC as a starting material, which was produced by carbothermal reduction of silica in argon atmosphere.

Formation of Si_3N_4 and SiC by reactions (1) and (2) under standard conditions needs a temperature above 1820K and 1788K, respectively (calculated using thermodynamic data from NIST-JANAF Thermochemical Tables). However, the reactions take place at lower temperatures under decreased CO partial pressure in a continuously flowing gas.

Conversion of SiC to Si_3N_4 via reaction (3) is thermodynamically favoured at lower reaction temperatures. The calculated equilibrium temperature for this reaction under standard conditions is 1715K. In our experiments, conversion of SiC to Si3N4 was observed at higher temperatures, 1723K and 1773K, what indicates that the

thermodynamic data at high temperatures are not reliable. Reaction (4) is thermodynamically unfeasible under experimental conditions of this work.

Reduction of silica also involves formation of SiO (silicon monoxide) as a gas intermediate:

$$SiO_{2(s)} + C_{(s)} = SiO_{(g)} + CO_{(g)} \quad (5)$$

$$SiO_{2(s)} + CO_{(g)} = SiO_{(g)} + CO_{2(g)} \quad (6)$$

SiC and Si_3N_4 can be formed by further reactions of SiO with carbon and carbon and nitrogen:

$$3SiO_{(g)} + 3C_{(s)} + 2N_{2(g)} = Si_3N_{4(s)} + 3CO_{(g)} \quad (7)$$

$$SiO_{(g)} + C_{(s)} = SiC_{(s)} + CO_{(g)} \quad (8)$$

Reaction (8) thermodynamically is more preferable than reaction (7). This is consistent with the observation that SiC was the main reduction product in the early stage.

It can be concluded that formation of silicon nitride by carbothermal reduction in a nitrogen atmosphere starts with the formation of SiO gas by reaction (5). SiO reacts with graphite to form SiC which is further converted to silicon nitride by reacting with nitrogen (reaction (3)).

Addition of hydrogen to the nitrogen gas promoted the carbothermal reduction of silica. When hydrogen was present in the gas phase, it formed methane, which acted as a reductant as shown in reactions (9) and (10):

$$2H_{2(g)} + C_{(s)} = CH_{4(g)} \quad (9)$$

$$SiO_{2(s)} + CH_{4(g)} = SiO_{(g)} + CO_{(g)} + 2H_{2(g)} \quad (10)$$

In this study, the optimal N_2-H_2 gas mixture in the carbothermal reduction contained 10 vol% hydrogen.

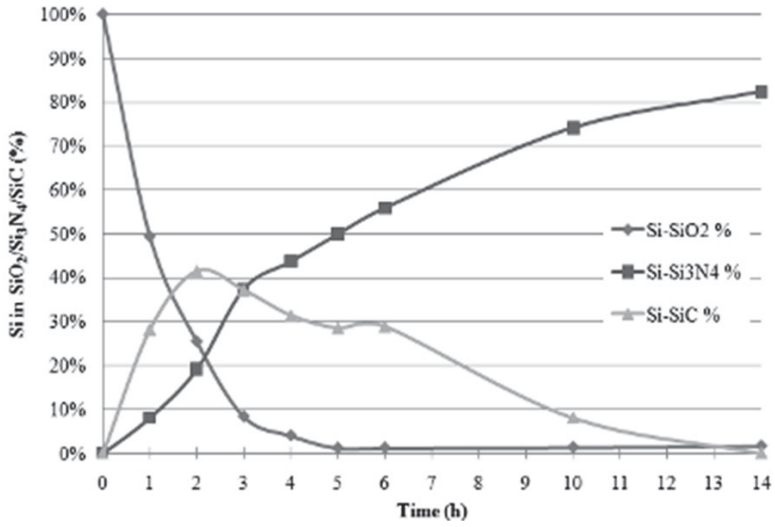

Figure 1. Distribution of silicon among SiO_2, Si_3N_4, and SiC in the progress of reduction at 1723K in 10% H_2- 90% N_2 gas mixture with a total gas flow rate at 1 NL/min.

A study of tin-based systems for E-waste processing

X.Xu, E.Jak, P. Hayes
Pyrometallurgy Research Centre, University of Queensland, Brisbane, Australia

With the continuously increasing amount of E-waste scrap in the world and the use of lead-free solder materials, the need to develop a suitable process for the recovery of these precious metals (Cu, Sn and Ag, Au, PGM's) is becoming a critical issue. The chemistry of primary tin smelting is mainly described by the seven component system SnO-SnO_2-FeO-Fe_2O_3-CaO-Al_2O_3-SiO_2, which represents the logical starting point for the development of tin smelting for E-waste. A critical review on the phase equilibria on the tin-containing systems has shown, however, that the phase equilibria in these systems are not well defined.

The experimental method used in the present study involves high temperature equilibration/quenching/EPMA experimental procedures using the primary phase as a substrate. With these techniques, the following phase equilibrium investigations and liquidus determinations have been carried out:

1) The "SnO"-CaO-SiO_2 system at tin saturation

Experimental studies have been conducted to determine phase equilibria in the "SnO"-CaO-SiO_2 system in equilibrium with tin metal in the temperature range of 1148-1673 K. The melting temperature of SnO in equilibrium with tin metal was found to be between 1398 and 1403 K. The phase diagrams were constructed for the "SnO"-SiO_2 binary and "SnO"-CaO-SiO_2 ternary systems in equilibrium with tin metal. The eutectic in the "SnO"-SiO_2 binary is at 28.5 wt% SiO_2 and 1163K.

In the ternary section "SnO"-CaO-SiO_2 the liquidus temperatures have been determined in the tridymite, cristobalite, wollastonite, pseudo-wollastonite and cassiterite primary phase fields. The high melting temperature of pseudo-wollastonite and tridymite phases dominate the phase fields of the "SnO"-CaO-SiO_2 system. The CaO/SiO_2 ratio has a significant effect on the liquidus in the "SnO"-CaO-SiO_2 system. One ternary eutectic has been established involving the formation of tridymite, malayaite and cassiterite primary phases. Five ternary peritectic reactions have been identified.

2) The "SnO"-SiO_2-"FeO" system at Sn-Fe alloy saturation

The primary phases and liquidus temperatures in the "SnO"-"FeO" binary and "SnO"-SiO_2-"FeO" ternary systems in equilibrium with tin-iron alloy between 1148 and 1673 K, have been experimentally determined. The following primary phase fields were identified including FeO_x (wustite), $Fe_{(3-x)}Sn_xO_4$ (Spinel, $0.34<x<0.59$), Fe_2SiO_4 (fayalite), SiO_2 (tridymite), $Fe_4Si_2Sn_7O_{16}$ (tin iron silicate), and SnO_2 (cassiterite). Several invariant points were identified in the "SnO"-SiO_2-"FeO" system, including two ternary eutectic points and three ternary peritectic points.
It was also found that the most striking feature in the system is the extent of the low temperature melting region across the complete range of compositions from the "SnO"-SiO_2 to the "FeO"-SiO_2 binary system. There are no high melting temperature ternary compounds in the system at alloy saturation.